Authors' response to reviewer #1's comments

Specific comments 1) It is well established that quartz fiber filters (such as the front filter used to collect particles) adsorb organic vapors quite well. Was anything done in this study to evaluate the effect of this on the results and data interpretation? If not, then I suggest some vapors of standard PAHs with a range of volatilities be sampled and analyzed using this system. Alternatively, if others have conducted such studies then the authors could review the results of that work and discuss its consequences for the sampling and measurement approach employed here.

Authors' response to specific comment 1):

We thank the reviewer for his/her suggestion of discussing the consequences of the adsorption of organic vapors onto the filters in our two-filter sampling system and measurement approach. We will make sure that this possibility is acknowledged and briefly explain why we are confident that this phenomenon does not affect our results in a revised version of our manuscript. Please find our detailed response below.

The reviewer is right that the adsorption of gaseous hydrocarbons onto filters was investigated in numerous works. Specific studies assessing the ability of various filters to sorb gaseous organic species have even been carried out [e.g. 1-5]. They show that filters can collect organic vapors in addition to particulate matter. The efficiency of the adsorption of such vapors depends on a number of factors, including sampling duration and gas flow through the filter. In our study we used two filters placed in series in the exhaust line of a miniCAST, i.e. a bare quartz fiber filter (front filter) followed by a second black-carbon-covered quartz fiber filter (back filter). By doing so, we observed after a short sampling time (20 min) a clear partitioning where the particulate matter is essentially found on the first filter, while organic vapors (i.e. polycyclic aromatic hydrocarbons (PAHs) of different masses) are found condensed either onto both filters or just onto the back filter depending upon the masses of the PAHs.

Prior to sampling, spectra of neat quartz fiber filters (QFFs) have been recorded for both L2MS and SIMS measurements. The thermal treatment applied to the back filter proved to be very efficient at limiting the adsorption of aromatic species as evidenced when comparing the mass spectra of the quartz fiber filters before and after exposure to the exhaust. Moreover, the masses retained from our front and back filters to per-form statistical analyses do not include specific masses associated with the substrate. Therefore, none of our deduction from statistical analysis is impacted by the possible condensation of organic vapors.

During our experiment, adsorption of organic vapors on the filters could affect the chemical characterization of the particulate matter if we were using an analytical technique probing the bulk of the sample, i.e. from the sample surface all the way down to the filter. For instance, it is true that the adsorption of gaseous organic compounds onto filters is a potential source of errors in measurement when determining the mass of collected particles and the concentration of certain species/organic carbon (OC) in the particulate phase with a thermo-optical method [3-5]. However, in this work, we use instead two-step laser mass spectrometry (L2MS). L2MS is a surface characterization technique; since the laser penetration depth atλd=532 nm is only a few nm (orders of magnitude smaller than the average particle size in the studied regimes) only species present on the surface of the particulate matter are desorbed and analyzed. Therefore, if organic vapors are adsorbed onto the filter, they should not induce any measurement artifact when analyzing the particulate matter. This does not mean that organic vapor did not condense onto the particulate matter. We acknowledge and mention in the main text of our article that particulate matter likely consists of an adsorbed layer of organics onto an elemental carbon core. However, our experiment has not been de-signed to identify for certain whether heavy PAHs (>4 rings) are part of the particulate matter (chemisorbed or physisorbed) or “free” in the gas phase, insofar as they are both concomitantly present in the exhaust line and that we cannot avoid the fact that heavy PAHs may condense along with/onto the particulate matter when the latter is trapped by the first filter.

Authors’ changes in the manuscript:

More detailed and complementary answers to specific comment 1 can be found in the authors’ response to specific comments 1, 3, and 4 of Referee #2. In particular, we specify the changes we wish to make in the main text to fully address this comment.

2) I found the Results and Discussion section rather challenging to read, due primarily to the somewhat monotonous style in which each observation was de-scribed in detail and then a possible explanation was provided. This made it difficult for me to differentiate important observations from minor ones. Although this made for a very thorough presentation, I’m not sure that readers will get the important take-away messages until they read the Conclusions (which may be all they choose to fully read). I suggest that the authors make a greater effort to emphasize the major points in each section of the manuscript, and perhaps eliminate some of the discussion that is mostly just minor observations with speculative explanations.

Authors’ response to specific comment 2):
We will follow the reviewer’s comment and improve the Results and Discussion section of our article in a revised version where we will outline the most important observations for each paragraph and remove extended descriptions/discussions about less important points that currently disrupt the thread.

Authors’ changes in the manuscript:

Changes in the main text answering specific comment 2 are detailed in the authors’response to specific comments 8 and 9 of Referee #2. More specifically, we outlined the most important observations and conclusions of the Results and Discussion section. We rewrote to a great extent sections 3.1.2 and 3.2.2. to improved the overall readability of our article.

Technical comment 1) Line 46: It seems unlikely that reviews published in 2011 and 2014 cover advances made over the last decade. Sentence should be reworded.

Authors’ response to technical comment 1): The sentence on line 46 will be reworded in our revised version. We will additionally replace “decade” by “decades” and add a more recent reference.

References:

1. Chase R., Duszkiewicz G., Richer, J., Lewis D., Maricq M., and Xu N., "PM Measurement Artifact: Organic Vapor Deposition on Different Filter Media," SAE Technical Paper, 2004, 2004-01-0967, 1-11.
2. Cotham W. E., and Bidlemant T. F., “Laboratory Investigations of the Partitioning of Organochlorine Compounds between the Gas Phase and Atmospheric Aerosols onGlass Fiber Filters”, Environ. Sci. Technol., 1992, 26, 469-478.

3. Hartt K. M., and Pankow J. F., “High-Volume Air Sampler for Particle and Gas Sam-pling. 2. Use of Backup Filters To Correct for the Adsorption of Gas-Phase Polycyclic Aromatic Hydrocarbons to the Front Filter”, Environ. Sci. Technol., 1994, 28, 655-661.

4. James J. Schauer, Michael J. Kleeman, Glen R. Cass, and Bernd R. T. Simoneit,"Measurement of Emissions from Air Pollution Sources. 2. C1 through C30 Organic Compounds from Medium Duty Diesel Trucks", Environ. Sci. Technol., 1999, 33 (10),1578- 1587.

5. Mader B. T., and Pankow J. F., “Gas/Solid Partitioning of Semi-volatile Organic Com-pounds (SOCs) to Air Filters. 3. An Analysis of Gas Adsorption Artifacts in Measurements of Atmospheric SOCs and Organic Carbon (OC) When Using Teflon Membrane Filters and Quartz Fiber Filters”, Environ. Sci. Technol., 2001, 35(17), 3422-3432.

Authors' response to reviewer #2's comments

We would like to thank the referee for his/her careful reading of the manuscript and the detailed comments that were provided. We think we addressed all the referee's concerns and we edited our manuscript when further details or clarifications were needed.

1) **Collection system and experimental set-up. The collection system poses some serious problems. Positive artefacts are well known on quartz filters. Some of the filters were highly charged (PF1, PF2, PF3). We could expect that a kind of "soot cake" is formed on the front filters increasing the filtration efficiency and causing more adsorption of the gaseous compounds onto the deposited particles (see Fig. 1 images front filters).**

Authors' response to comment 1):

The referee explains that the trapping of particulate matter on the first filter could subsequently increase the filtration efficiency and therefore cause more gaseous compounds to adsorb onto the particles.

While the referee's comment is true, another artefact is also reported in the literature: species originally adsorbed on the PM can also desorb during sampling and be retained on the back filter, which would lead to an overestimation of the gas-phase fraction (Paolini et al., 2017).

We acknowledge and mention in the main text of our article that particulate matter likely consists of an adsorbed layer of organics onto an elemental carbon core (e.g. abstract l.19 or p.4, l. 117: "*In the present study, the sampling line was designed to collect PM (including adsorbed species) on the Front Filter [...]*"). Our experiment has not been designed to identify for certain whether heavy PAHs are part of the particulate matter (chemisorbed or physisorbed) or "free" in the gas phase, insofar as they are both concomitantly present in the exhaust line and that we cannot avoid the fact that heavy PAHs may condense along with/onto the particulate matter when the latter is trapped by the first filter. However, what our experimental set-up reveals is that different classes of compounds are almost solely found on each of the two filters. To highlight this observation, a "contrast function" defined as the $\frac{S_{FF}-S_{BF}}{S_{FF}+S_{BF}}$ ratio is represented for the 266 nm L2MS data in Fig. 1, where S_{FF} and S_{BF} are to the ion signals associated to a mass peak detected on the Front and the Back Filters. This representation clearly outlines that small aromatic species are found solely on Back Filters, whereas large PAHs are mostly on Front Filters. This suggests that the lightest species do not condense significantly onto the first filter and do pass through. As what we referred to as semi-volatiles are found on both filters, it is indeed possible that PAHs included in that category are affected by an increased filtration efficiency of the first filter due the concomitant particulate matter adsorption (thus forming a thick soot deposit). This would result in a lower concentration of these PAHs on the back filter with respect to the front one, which would appear in our data as a lower absolute intensity of the corresponding mass peaks. However, this effect would not affect the covariance between mass peaks *(m/z)* as similar diffusion behaviors can be expected within SP1 and SP3 samples, for instance, because of similar soot porosity (e.g. the porosity of the soot "cake" deposited on silicon wafers for SP1 and SP3 set points were calculated to be about 98.1% and 97.4 %, respectively, Ikhenazene et al., 2019). We therefore expect from a statistical standpoint that for each detected mass peak (*m/z*), the covariance will only negligibly be affected by diffusion.

Author's changes in the manuscript:

We first acknowledged this possibility in the article (page 4, line 118) by adding 2 sentences and the corresponding reference:

"*Note that particles build-up on the Front Filter could potentially increase its filtration efficiency and consequently trap PAHs that would rather pass through if the thickness of the PM collected on the Front Filter was not that high. Alternatively, species originally adsorbed on the PM can also be desorbed during the sampling and be retained on the back filter, which would lead to overestimate the gas-phase fraction (Paolini et al., 2017). However, our results will show that if this is the case, only specific PAHs of intermediate volatility are impacted by this phenomenon. In addition, this effect would not affect our statistical analysis (e.g. the covariance between mass peaks (m/z)) as similar diffusion behaviors can be expected within SP1 and SP3 samples, which exhibit similar soot porosity (e.g. the porosity of the soot material deposited on silicon wafers for SP1 and SP3 set points were calculated to be about 98.1% and 97.4 %, respectively, Ikhenazene et al., 2019). We therefore expect, from a statistical standpoint that for each given m/z, the covariance will only negligibly be affected by diffusion.*"

In addition, we introduced a figure and its description to demonstrate that some species are present specifically on either the Front Filter or the Back Filter, showing that the mentioned artefact is not dominant in our two-filter system for the non-volatile and volatile species, respectively (Fig. 4 in the main text and attached in copy to this Authors' response). The text page 9 line 261 reads now:

"The various CAST set points exhibit different PAH mass distributions on their Front and Back Filters, which likely relates to the different volatility properties of PAHs and probably affects their subsequent trapping on Front and Back Filters. Distinct volatility properties have been observed in the past on particles originating from wood combustion by Bari et al. (2010), who classified the PAHs on the basis of their number of aromatic rings resulting in the detection of three different PAHs categories. The authors classified the PAHs consisting of two aromatic rings as volatiles as they were mostly found in the gas phase, while those made of three and four rings were classified as semi-volatiles. PAHs comprising more than four rings were classified as non-volatile as they were observed in the PM in their study. Note that slightly different classes have also been defined in the literature (An et al., 2016; Elghawi et al., 2010; Sun et al., 2006). In our study, we largely found compounds consisting of one and two aromatic rings on Back Filters, while PAHs of m/z *176–242 were found on both Back and Front filters and those of* m/z *≥ 252 predominantly on Front Filters. Such PAH partitioning between Front and Back Filters is in line with the work of Bari et al. (2010). Similarly, we categorized the PAH distributions found on CAST samples into a volatile, semi-volatile, and non-volatile fraction (Fig. 3), where the volatile fraction encompasses here aromatic species made of one to two aromatic rings (*m/z *78–166), the semi-volatile fraction comprises PAHs with a mass range of* m/z *176–242, and the non-volatile fraction includes PAHs of* m/z *≥ 252. The boundaries of these intervals have been refined using the representation of Fig. 3 in which the "contrast function" defined as the* $\frac{S_{FF}-S_{BF}}{S_{FF}+S_{BF}}$ *ratio is represented for the 266 nm L2MS data, where* S_{FF} *and* S_{BF} *are to the ion signals associated to a mass peak on the Front Filter and the Back Filter respectively. This representation clearly outlines that small aromatic species are found solely on the Back Filters, whereas large PAHs are mostly on the Front Filters."*

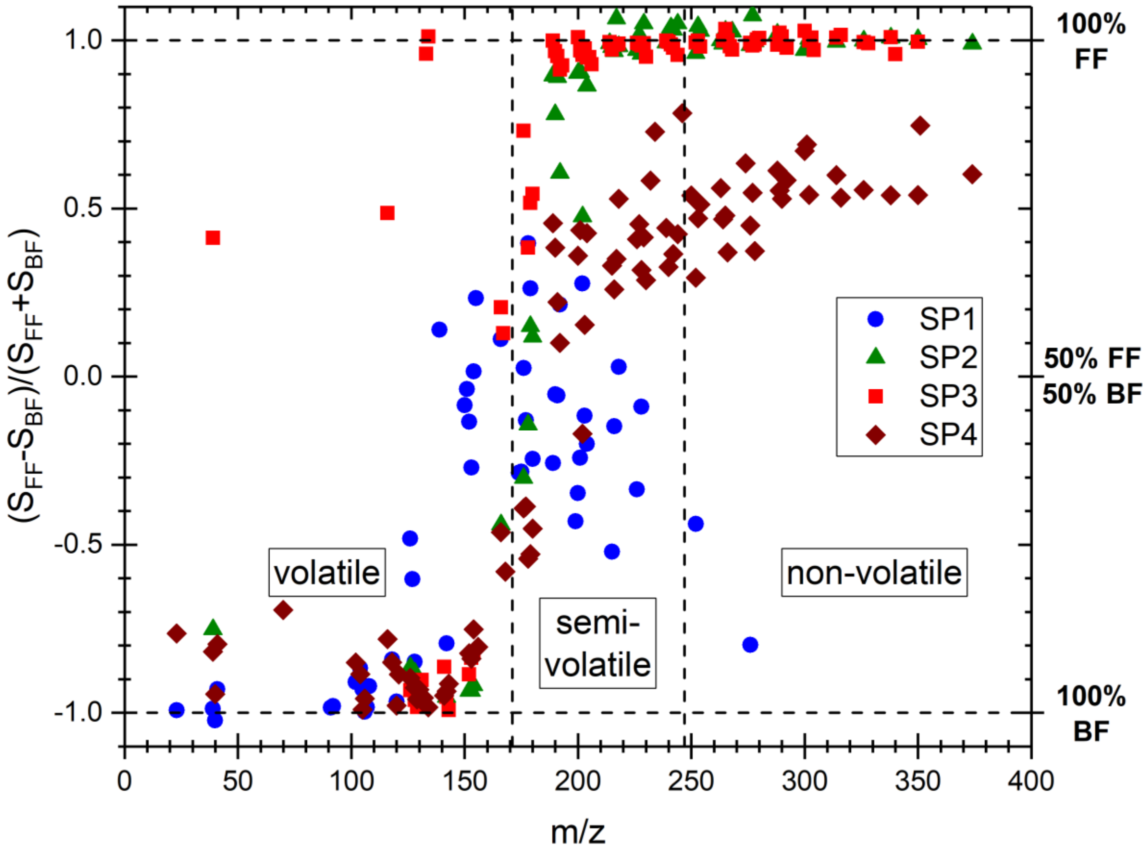

Figure 1. "Contrast plot" representing the variation in PAH signal detected with L2MS at λ_i = 266 nm for the 4 CAST set points. Values on the y-axis correspond to the partitioning of the species between the Front Filters and Back Filters: -1 indicates that the species are all found on the BF, +1 that they are all found on the FF, and 0 that they are equally partitioned on both filters.

2) **In fig. 2 front and back filters mass spectra (L2MS) are presented. The m/z 202 ion partition on both the gas and particle phases (for SP1, SP2, SP4 but not for SP3) even though the signal is very high in the mass spectrum of the particle phase it almost not visible in the gas phase. How is it possible if for the other SPi it did partition? So why the partitioning of m/z 202 is so different for SP3 with respect to the other?**

Authors' response to comment 2):
The referee is concerned about specific behaviors observed for SP3. In the literature, various analyses converge towards the fact that the SP3 set point is distinct from the others in that i) the organic to total carbon ratio is higher (87% versus ≤ 47% for the other setpoints) – information that we confirmed with via our mass spectrometry measurements of the total PAH content (see Fig. 3 and Fig. 6), and ii) the crystallites of the particles produced in these conditions are significantly smaller and form a distinct disordered arrangement exhibiting many carbon edges (Bescond et al., 2016; Marhaba et al., 2019; Ouf et al., 2016; Yon et al., 2015).

Such smaller crystallites suggest that SP3 may undergo nucleation and growth processes different from those of the other set points, thus leading to a different chemical composition for both particulate and gas phases.

The partitioning of SP3's *m/z* 202 ion between the Front and Back Filters is different from that of the other CAST set points. Specifically, the referee points out that, according to our L2MS mass spectrum, *m/z* 202 is almost exclusively found on the Front Filter in contrast to what is observed for SP1, SP2, and SP4. The partitioning of *m/z* 202 between FF and BF can be explained by thermodynamic and chemical considerations. First, it is useful to recall that mass spectrometry provides information about the mass of detected species (i.e. the chemical formula) but does not permit a direct determination of the structure of the detected molecules. In fact, for *m/z* 202 ($C_{16}H_{10}^+$), many different isomers (NIST Chemistry WebBook) can potentially contribute to the signal. The volatility of different isomers can vary, for instance the vapor pressure of fluoranthene is two times higher than that of pyrene (between 320K and 390 K, Goldfarb and Suuberg, 2008). The relative contribution of different isomers to the detected signal highly depends on combustion conditions (i.e. CAST set points) and therefore on the chemistry. The high signal at *m/z* 202 observed for the SP3 Front Filter can be explained by a much higher contribution from isomers with a lower volatility (e.g. pyrene) produced in this regime. Second, it is clear that the chemistry in the reactive medium and the nature of the soot particles produced in the different set points of the miniCAST can lead to a large diversity in the relative chemical composition of the particulate phase and the gas phase.

Author's changes in the manuscript:

To address the referee's concern, we now discuss this particularity of m/z 202 in the main text of our article. We added on page 8, l. 253 the following discussion:

"*Literature data converge towards the fact that the SP3 set point is distinct from the others in that i) the organic to total carbon ratio is higher (87% versus ≤ 47% for the other set points), and ii) the crystallites of the particles produced in these conditions are significantly smaller and form a distinct disordered arrangement exhibiting many carbon edges (Bescond et al., 2016; Marhaba et al., 2019; Ouf et al., 2016; Yon et al., 2015). Such smaller crystallites suggest that SP3 may undergo nucleation and growth processes different from those of the other set points, subsequently leading to distinct chemical compositions (e.g. different isomeric distributions) of the PM. The relative ion signals observed between the Front and Back Filters hence depend upon the relative volatilities and the response of the chemical compounds present on the samples to the 266 nm R2PI L2MS.*"

3) **Another issue is the dilution system and the temperature in the sampling line. Low dilution at room temperature will enhance adsorption of relatively light PAHs onto the particles, while once in the atmosphere high dilution will alter this partitioning. This aspect has not been addressed.**

Authors' response to comment 3):

The referee is concerned that the low dilution/room temperature conditions in the sampling line as those used in our experiment induce the preferential adsorption of light PAHs on soot particles.

For the sake of clarity, we would like to specify that the sole dilution system in our experimental setup is that of the miniCAST generator itself (dilution airflow 20 l min^{-1}, Fig. 1). We added a sentence on p.3, l.93 to make that fact clear: "*Note that the sole dilution system in our experimental setup is that of the miniCAST generator itself (dilution airflow 20 l min^{-1}, Fig. 1)*."

Some studies are interested in probing the particulate matter in a chemical state as close as possible as that generated during the combustion process. In order to do so, it is necessary to avoid as much as possible any coating (PAHs, water) that could result from the adsorption of gaseous species during the collection, and accordingly, it is common to use additional dilution stages and denuders. In contrast, the goal of this study is to fully characterize the particulate and gas phase of combustion by-products as they are emitted from the source, i.e. at the exhaust of a model soot generator without adding any dilution stage. We agree that the lower dilution of our sampling line plays on the partitioning of chemical species compared to systems having greater dilution factors. However, this phenomenon can be modeled (Lohmann and Lammel, 2004; Pankow, 1994) once the initial partitioning of chemical compounds (at the exhaust port) is known – information provided by this study. It is hence useful to characterize combustion by-products in the vicinity of the standardized source as it allows gathering data for subsequent simulations of the partitioning evolution in the atmosphere (at a different ambient temperature, air humidity, and pressure). In addition, Fig. 3 highlights that without using any extra dilution system, our two-filter approach is able to reproduce the separation commonly found in the literature regarding PAHs volatility properties, where the lightest are only found in the gas phase and do not condense on the PM collected on the Front Filters, and the non-volatile PAHs are predominantly found on the Front Filter.

Author’s changes in the manuscript:

We added a sentence on p.3, l.93 to specify that we did not use an extra dilution system: “*Note that the sole dilution system in our experimental setup is that of the miniCAST generator itself (dilution airflow 20 l min^{-1}, Fig. 1*).”

4) **It is relatively common, when working on filter samples, to remove the gaseous phase using denuders. This test has not be done apparently, and it would have been a easy test to verify the presence of organic volatile of the front filter.**

Authors’ response to comment 4):

As suggested by the referee, a commonly used approach for avoiding positive artifacts is the use of a denuder upstream of the quartz fiber filter to remove organic gases from the incoming air stream (e.g. Fitz, 1990). However, the removal of the organic gases also alters the gas-particle equilibrium and leads to a partial volatilization of the particle-bound organic phase, thus significantly changing the chemical composition of the particulate phase. Note that negative artifacts induced by the volatilization of species on the quartz fiber filter can also appear (Paolini et al., 2017). These artifacts can be accounted for, in particular for OC measurements of particulate matter, if the species that were vaporized are then trapped by an absorbing medium/filter (the total OC is the sum of OCs from two filters). However, since the efficiency of denuders is less than 100%, the gas phase will not only contain species that were vaporized from particles after the denuder but also a fraction of the original gas phase, and therefore the OC measured for the absorbing filter will be higher (positive artifacts). In other words, as the concentration of gas-phase organics is typically an order of magnitude higher than that of the particle-bound organic species, gas-phase material escaping the denuder can potentially create substantial positive sampling artifacts on the adsorbent backup filter (denuder breakthrough) (Subramanian et al., 2004). Sampling combustion by-products with the experimental system we propose, that is without a denuder, offers information about the unaltered gas and particulate phases, and therefore is more preferable to identify their presence on filters collected directly in the exhaust line, as is often the case in the literature (Crawford et al., 2011; Ess et al., 2016; Yon et al., 2015). Thermo-optical methods are often used to calculate the OC/TC ratio of CAST soot samples collected in the exhaust line. Our study provides information about the nature of the organic fraction and evidences the phase from which PAH molecules are most likely to originate. We do not exclude the condensation of the gas-phase on the particles once they are trapped by the Front quartz fiber filter, in fact, it is clear from the analysis of the two filters that PAHs classified as semi-volatile compounds and to a lesser extent as non-volatile compounds are found on both filters with the largest fraction on the Front Filter, which could possibly be indicative of a preferential adsorption on the particles. This shows also that there are indeed PAHs of intermediate volatility on the particulate matter trapped on the Front Filter. However, it is also clear from our analyses that the lightest PAHs are not found on the Front Filter, which suggests that when gas-phase condensation occurs, it does not affect significantly the fraction constituted of the lightest PAHs.

5) **Environmental relevance. The authors claim that their approach allows to identify distinct surface chemical compositions of aerosols discriminating semi-volatile and nonvolatile polycyclic aromatic hydrocarbon (PAH) contents as a function of the combustion process. However modern engines are equipped with after-treatment devices that highly alter the exhaust emissions (oxidation of hydrocarbons and particle bound compounds). So in which way these results can be extrapolated to nowadays diesel engine emissions?**

Authors' response to comment 5):
As stated by the referee, it is true that modern certified engines are equipped with after-treatment systems (e.g. particle filters, catalytic strippers) that significantly change the chemical composition of both phases (particulate and gas phase). In a recent study we showed that a catalytic stripper that complies with European regulations for PMP systems (> 99 % removal of ≥ 30 nm tetracontane particles) successfully removes the majority of particle-bound organic species (Focsa et al., 2019), and more specifically removed the volatile particles as well as the organic species from the surface of nonvolatile particles and subsequently increased the contribution of EC (carbon clusters) (Focsa et al., 2019). The proposed two-filter method can therefore be used to assess the efficiency of after-treatment systems by simultaneously measuring their impact on both particulate and gas phases.
Moreover, besides on-road vehicles (with certified engines), there are a large number of other sources of combustion by-products that do not have any after-treatment systems and for which our analyses are relevant. Aircraft jet engines, wood combustion stoves, biomass burning are just a few sources of combustion by-products whose exhaust is not subjected to an active after treatment system. Therefore, using a miniCAST soot generator operated with different parameters as a source of combustion by-products, which can mimic some of the physico-chemical properties of aircraft emissions for instance (Bescond et al., 2014; Marhaba et al., 2019; Moore et al., 2014), allows for potential real-world extrapolations of our results for combustion devices not equipped with after-treatment systems. The proposed method of sampling and characterizing concomitantly the particulate and gas phases can thus be extremely useful when evaluating the impact of these sources on the environment, as the gas/particulate portioning conditions the overall reactivity. As a perspective it would be very interesting test the efficiency of such devices especially when the engine starts.

Author's changes in the manuscript:

To account for the referee's comment we modified the original sentence, which now reads:

“The CAST (Combustion Aerosol Standard) generator is often chosen to produce combustion-generated particles as it is easy to implement for systematic laboratory experiments with the fuel and oxidation air flows being easily modifiable, and hence enables the investigation of a variety of chemistries. Therefore, using a miniCAST soot generator operated with different parameters as a source of combustion by-products, which can mimic some of the physico-chemical properties of aircraft emissions for instance (Bescond et al., 2014; Marhaba et al., 2019; Moore et al., 2014), allows for potential real-world extrapolations of our results for combustion devices not equipped with after-treatment systems. The proposed method of sampling and characterizing concomitantly the particulate and gas phases can thus be extremely useful when evaluating the impact of various sources (aircraft jet engines, wood combustion stoves, biomass burning) on the environment, as the gas/particulate partitioning conditions the overall reactivity. As it can simultaneously measure the particulate and gas phases, the proposed two-filter method can therefore be utilized to assess the efficiency of after-treatment systems, which are known to successfully remove the majority of particle-bound organic species (Focsa et al., 2019), and more specifically to remove the volatile particles and the organic species from the surface of nonvolatile particles while increasing the contribution of EC (carbon clusters) (Focsa et al., 2019).”

6) **Quantification issues: since the author states that using three different ionization wavelengths, it is possible to target various classes of compounds and to reach sub-fmol limit of detection, e.g. for PAHs (Faccinetto et al., 2008, 2015). So why the results are not present in a quantitative way?**

<u>Authors’ response to comment 6)</u>:
The referee refers to the sentence on page 3, l. 77: “Using three different ionization wavelengths, it is possible to target various classes of compounds and reach sub-fmol limit of detection, e.g. for PAHs (Faccinetto et al., 2008, 2015).”

Semi-quantitative results can be obtained with L2MS using external standards (synthetic soot), which consist of black carbon covered with chemical compounds whose surface concentration is well defined, and to which the signal collected in a sample can be compared (see Faccinetto et al., 2011, 2015) for a detailed description of the procedure). This approach can be used for PAHs exhibiting little to no fragmentation upon desorption and ionization, and is consequently more delicate to implement for aliphatic compounds, which undergo greater fragmentation after laser ionization (e.g. 118 nm). Moreover, this quantification step is complexified in the case of real soot by the presence of multiple PAH isomers for the same molecular formula. Such quantification study is out of the scope of the present paper but will be in our priorities for future publications. Here we are only providing information about the chemical species present on the sample surface and their relative contribution with respect to their volatility. The limit of detection corresponds to the minimal desorbed amount of a specific compound that results in a detectable signal. Even though the limit of detection has been already measured for various PAHs (Faccinetto et al., 2011, 2015), this information cannot be used for quantification purposes. The limit of detection changes from isomer to isomer, therefore, for a reliable quantification, the relative contribution of all present isomers should be known – information that cannot be retrieved only from mass spectra. Since we are using desorption and ionization conditions akin to those described in Faccinetto et al. (2015), we assume that our detection limit is similar.

<u>Author’s changes in the manuscript:</u>

To account for the reviewer’s comment and dissociate the ideas of quantitative results and detection limit, we modified the sentence page 3, l. 77, which now reads:

"*Using three different ionization wavelengths, it is possible to target various classes of compounds such as aromatic and aliphatic compounds. In addition, it is possible to reach a sub-fmol limit of detection for PAHs upon specific desorption and ionization conditions* (Faccinetto et al., 2011, 2015)."

7) **Preparation of the filters. Prior to sampling the authors prepared the filters by heating them at 150_C for 16 hours. It seems to be a relatively low temperature with respect to the common procedure found in the literature for quartz filters (often up to 400_C).**

Authors' response to comment 7):
The preparation procedure described above was primarily used to remove the pre-adsorbed species from the black carbon layer. The referee points out that the temperature of 150°C is lower than that commonly used (400°C). While this is true, all filters (bare quartz fiber filters and carbon-covered quartz fiber filters) have been analyzed in L2MS using the aromatic-selective 266 nm wavelength and in SIMS before they were placed in the exhaust line. As no signal could be evidenced in L2MS and only negligible signal was recorded in SIMS, we believe that our pre-treatment procedure prevented the adsorption of any unwanted compounds. In addition, it is worth recalling that the mass spectrometry techniques that we use are surface sensitive, which means that the signal we recover from Front and Back filters is that of the uppermost layer and thus for such thick samples our results are not affected by the composition of the substrate before sampling.

8) **Poor English and paper structure. The paper is far too long and should be reduced in length and simplified. We need to understand what is important and not and to get few strong messages expressed in a clear and synthetic way. This paper is written as a scientific report or a student PhD thesis. I strongly suggest to revise completely the paper and possibly make nicer figures and plots.**

Authors' response to comment 8):

We followed the referee's comment and improved the Results and Discussion section of our article in where we outlined the most important observations and shortened the extended descriptions. Specifically, we added 2-3 lines of conclusion at the end of each section (namely sections 3.1.1., 3.1.2., 3.2.1., 3.2.2.), we rewrote to a great extent sections 3.1.2 and 3.2.2. to outline the main findings, and we turned some supporting materials to supplementary information (PCA for 157 nm and 118 nm). We think these changes improved the overall readability of our article. In addition, we greatly improved figures quality in order to make them clearer and nicer. Finally, the article will be read and corrected by a native English speaker before submission of the revised version. However, we do think that the actual length of our article is necessary to fully describe the comprehensive analyses that we performed.

Author's changes in the manuscript:

Please refer to our response to comment number 8) for the short description of our changes or to the main text for detailed information.

9) **PAC analysis. The added value was "to highlight variation and patterns in a data set, and in this case was used to reveal the differences in chemical composition of the samples, and in particular**

between (i) Front and Back Filters and (ii) miniCAST set points." I can only partly agree to the added value of PCA analysis nevertheless the discussion is far too long. Please revise it.

Authors' response to comment 9):
We recently showcased the advantages of using advanced statistical techniques (Duca et al., 2019; Irimiea et al., 2018, 2019) to highlight subtle differences in the chemical composition of various samples. It is also very useful to confirm initial trends deduced from a descriptive approach of the mass spectra with a more quantitative approach such as that provided by the statistical analyses. However, to make the paper clearer and more synthetic, we did move PCA for 118 and 157 nm L2MS data to the supplementary information. PCA discussions for 266 nm L2MS and SIMS data have been rewritten to highlight the main conclusions and added values of these analyses.

Author's changes in the manuscript:
Subsections 3.1.2 and 3.2.2. have been rewritten as follows:

*"**3.1.2 Principal component analysis of L2MS spectra***

In order to better discriminate the chemical composition of the various samples, particularly (i) the Front and Back Filters and (ii) the miniCAST set points, principal component analysis (PCA) was applied to mass spectra recorded for all three individual ionization wavelengths. A full description of this statistical method is provided in Sect. S2. Here, the covariance matrix was built from the integrated areas of all the detected peaks with a signal-to-noise ratio SNR > 3. The physical meaning of all derived principal components can be inferred from the contribution of the various molecular species to the loadings (see Sect. S2 and Fig. 5b and S3). By identifying the molecular families contributing to this variance, we can interpret the PCA score plots (Fig. 5) and grasp the nature of the subtle chemical differences between the samples.
In L2MS data generated with 266 nm ionization wavelength, the scree and loading plots presented in Fig. 5b and S2a, respectively, show that PC1 expresses the largest variance (58.86 %) in the dataset and differentiates samples represented by a greater amount of high-mass PAHs (positive contribution: $m/z \geq 189$) from those containing more of low-mass aromatic species (negative contribution: up to three aromatic rings), especially naphthalene (m/z 128). PC2 (19.30 %) denotes the relative contribution between high-mass PAHs (positive contribution: $m/z \geq 216$) bearing four and more aromatic rings and aromatic compounds containing up to m/z 202, especially m/z 178 and 202, and benzene and its alkyl-derivatives. The dataset, in terms of PC1 and PC2, is illustrated in a score plot in Fig. 5a. According to PC1, the largest separation appears between sample groups $SP2\text{–}4_{FF}$ and $SP1\text{–}4_{BF}$. It can be attributed to the greater amount of high-mass PAHs ($m/z \geq 189$) relative to smaller aromatic species for the former group compared to the latter. The first conclusion is that our samples are mainly separated regarding their chemical composition (non-volatile and semi-volatile fractions vs volatile fraction) because of the two-filter collection system rather than the CAST operating conditions. However, a refined observation in the PCs can help to interpret composition variations between the different set points. For Back Filters, the PC1 score decreases along with the oxidation air flow indicating a greater contribution of small aromatic species, especially naphthalene, for lower oxidation air flows. Data points for Front Filters generally display a positive PC2 component except for $SP1_{FF}$, a phenomenon possibly explained by the very small fraction of non-volatile PAHs produced in this regime relatively to m/z 178 and 202. This almost constant score of PC2 for $SP2\text{–}4_{FF}$ on one hand, which is in contrast with the very different scores for the Back Filters (Fig. 5a), and the high contribution of semi-volatile species to the PC2 loadings (Fig. 5b) highlights that the ratios of semi-volatile compounds vary between the Front and Back Filters for the different set points. This observation demonstrates that the partitioning between the Front and Back Filters is not only driven by thermodynamic conditions (volatility) but also on the nature of the soot matrix produced at the different set points. Note that details about the PCA applied to the 157 nm and 118 nm L2MS data can be found in the supplementary material. The statistical approach developed in this section confirms from a quantitative standpoint the descriptive results obtained in Sect. 3.1.1. "

*"**3.2.2 Principal component analysis of SIMS spectra***

PCA was applied to the positive mode SIMS spectra. All hydrocarbon fragments and the most representative peaks for PAHs were chosen for the analysis (see Sect. S3 and Fig. S4). The PCA score plot for the first two components (PC1 and PC2, responsible for 92 % of the variance) is presented in Fig. 9a, and their corresponding loadings in Fig. 9c. PC1 represents 73 % of the variance and is associated with small fragment ions with m/z < 160 (e.g. $C_nH_3^+$ with n = 1–3, $C_nH_m^+$ with m > n, $C_7H_7^+$, positive coefficients), and with polyaromatic species with m/z ≥ 165 (negative coefficients). All Back Filter samples (containing gas-phase PAHs) but $SP4_{BF}$ have positive PC1 scores, whereas all Front Filters but $SP1_{FF}$ exhibit negative PC1 scores due to their high PAH contents. From this result, it can be determined that $SP3_{FF}$ has the highest relative PAH content. Among Front Filters, $SP1_{FF}$ has the smallest contribution from PAHs. $SP3_{BF}$ has the highest contribution from fragments associated with both aliphatic and aromatic species. The negative contribution of PC2 (19 % of the variance) is associated with the hydrogen-poor fragments ($C_nH_m^+$ with m < n) and volatile and semi-volatile PAHs (m/z 128–228) with the exception of m/z 165. The positive coefficients of PC2 are associated with aliphatic fragments (e.g. $C_nH_m^+$ with m > n) and large PAHs (m/z ≥ 239). As most of the variance was contained in only two principal components (92 %), there are only two available criteria for differentiating between samples: PC1, corresponding to the amount of PAHs relative to fragments, and PC2, depending partially on the hydrogen content of fragments originating from aromatic and aliphatic species. $SP1_{FF}$ and $SP1_{BF}$ are located in almost the same position due to their positive scores in PC1 and negative scores in PC2 that corresponds to their limited high-mass PAH content and high fragment content on one hand, and small PAHs and hydrogen-rich fragments on the other hand.

PCA was also applied to the negative mode SIMS spectra for selected mass peaks, including carbon clusters C_n^-, C_nH^-, and some oxygenated and nitrogenated fragment ions. The first two components were determined to represent more than 85 % of the variance. The score plot of PC1 vs PC2 is presented in Fig. 9b, along with their corresponding loadings (Fig. 9d). The first component, which accounts for over 67 % of the variance, separates the samples containing low-mass carbon clusters C_n^- (with n ≤ 3), nitrogen and oxygen bearing compounds (e.g. CN^-, C_3NH^-, CH_3O^-) (positive PC1) from the samples containing species with a higher mass ($C_nH_{0–2}^-$ with n ≥ 4, oxygenated, and nitrogenated fragments – negative contribution). The opposite contributions to PC1 of small carbon clusters in comparison to larger ones, with a transition size of n = 3–4, strengthen their dichotomous origin as already discussed in Sect. 3.2.1. In the light of the score plots, $SP1_{FF}$ and $SP1_{BF}$ samples are characterized by low surface coverages where small carbon clusters are associated with the soot matrix and the black carbon respectively, whereas the other samples are featured by PAH-rich surfaces. PC2, accounting for 18 % of the variance, separates data points based on the contribution from hydrocarbon compounds ($C_nH_m^-$, negative PC2) and oxygen/nitrogen bearing fragments (positive contribution). PC2 distinguishes $SP3_{BF}$, and $SP2_{BF}$ to a lesser extent, by their coverage in oxygen and nitrogen-containing species.

PCA on SIMS results confirm the existence of various families of carbon clusters on the PM that can be associated either with the soot matrix or the surface PAH coating.“

References

An, Y. Z., Teng, S. P., Pei, Y. Q., Qin, J., Li, X. and Zhao, H.: An experimental study of polycyclic aromatic hydrocarbons and soot emissions from a GDI engine fueled with commercial gasoline, Fuel, 164, 160–171, doi:10.1016/j.fuel.2015.10.007, 2016.

Bari, M. A., Baumbach, G., Kuch, B. and Scheffknecht, G.: Particle-phase concentrations of polycyclic aromatic hydrocarbons in ambient air of rural residential areas in southern Germany, Air Qual. Atmos. Heal., 3(2), 103–116, doi:10.1007/s11869-009-0057-8, 2010.

Bescond, A., Yon, J., Ouf, F. X., Ferry, D., Delhaye, D., Gaffié, D., Coppalle, A. and Rozé, C.: Automated Determination of Aggregate Primary Particle Size Distribution by TEM Image Analysis: Application to Soot, Aerosol Sci. Technol., 48(8), 831–841, doi:10.1080/02786826.2014.932896, 2014.

Bescond, A., Yon, J., Ouf, F.-X., Rozé, C., Coppalle, A., Parent, P., Ferry, D. and Laffon, C.: Soot optical properties determined by analyzing extinction spectra in the visible near-UV: Toward an optical speciation according to constituents and structure, J. Aerosol Sci., 101, 118–132, doi:10.1016/J.JAEROSCI.2016.08.001, 2016.

Crawford, I., Möhler, O., Schnaiter, M., Saathoff, H., Liu, D., McMeeking, G., Linke, C., Flynn, M., Bower, K. N., Connolly, P. J., Gallagher, M. W. and Coe, H.: Studies of propane flame soot acting as heterogeneous ice nuclei in conjunction with single particle soot photometer measurements, Atmos. Chem. Phys., 11(18), 9549–9561, doi:10.5194/acp-11-9549-2011, 2011.

Duca, D., Irimiea, C., Faccinetto, A., Noble, J. A., Vojkovic, M., Carpentier, Y., Ortega, I. K., Pirim, C. and Focsa, C.: On the benefits of using multivariate analysis in mass spectrometric studies of combustion-generated aerosols, Faraday Discuss., doi:10.1039/C8FD00238J, 2019.

Elghawi, U. M., Mayouf, A., Tsolakis, A. and Wyszynski, M. L.: Vapour-phase and particulate-bound PAHs profile generated by a (SI/HCCI) engine from a winter grade commercial gasoline fuel, Fuel, 89(8), 2019–2025, doi:10.1016/J.FUEL.2010.01.002, 2010.

Ess, M. N., Ferry, D., Kireeva, E. D., Niessner, R., Ouf, F. X. and Ivleva, N. P.: In situ Raman microspectroscopic analysis of soot samples with different organic carbon content: Structural changes during heating, Carbon N. Y., 105, 572–585, doi:10.1016/j.carbon.2016.04.056, 2016.

Faccinetto, A., Thomson, K., Ziskind, M. and Focsa, C.: Coupling of desorption and photoionization processes in two-step laser mass spectrometry of polycyclic aromatic hydrocarbons, Appl. Phys. A Mater. Sci. Process., 92(4), 969–974, doi:10.1007/s00339-008-4605-0, 2008.

Faccinetto, A., Desgroux, P., Ziskind, M., Therssen, E. and Focsa, C.: High-sensitivity detection of polycyclic aromatic hydrocarbons adsorbed onto soot particles using laser desorption/laser ionization/time-of-flight mass spectrometry: An approach to studying the soot inception process in low-pressure flames, Combust. Flame, 158(2), 227–239, doi:10.1016/j.combustflame.2010.08.012, 2011.

Faccinetto, A., Focsa, C., Desgroux, P. and Ziskind, M.: Progress toward the Quantitative Analysis of PAHs Adsorbed on Soot by Laser Desorption/Laser Ionization/Time-of-Flight Mass Spectrometry, Environ. Sci. Technol., 49(17), 10510–10520, doi:10.1021/acs.est.5b02703, 2015.

Fitz, D. R.: Reduction of the Positive Organic Artifact on Quartz Filters, Aerosol Sci. Technol., 12(1), 142–148, doi:10.1080/02786829008959334, 1990.

Focsa, C., Duca, D., Noble, J. A., Vojkovic, M., Carpentier, Y., Pirim, C., Betrancourt, C., P., Desgroux, Tritscher, T., Spielvogel, J., Rahman, M., Boies, A., Lee, K. F., Bhave, A. N., Legendre, S., Lancry, O., Kreutziger, P. and Rieker, M.: Multi-technique physico-chemical characterization of particles generated by a gasoline engine: towards measuring tailpipe emissions below 23 nm, Atmos. Environ., 2019.

Goldfarb, J. L. and Suuberg, E. M.: Vapor Pressures and Enthalpies of Sublimation of Ten Polycyclic Aromatic Hydrocarbons Determined via the Knudsen Effusion Method, J. Chem. Eng. Data, 53(3), 670–676, doi:10.1021/je7005133, 2008.

Ikhenazene, R., Pirim, C., Noble, J. A., Irimiea, C., Carpentier, Y., Ortega, I. K., Ouf, F.-X., Focsa, C. and Chazallon, B.: Ice Nucleation Activities of Carbon-Bearing Materials in Deposition Mode: From Graphite to Airplane Soot Surrogates, J. Phys. Chem. C, acs.jpcc.9b08715, doi:10.1021/acs.jpcc.9b08715, 2019.

Irimiea, C., Faccinetto, A., Carpentier, Y., Ortega, I. K., Nuns, N., Therssen, E., Desgroux, P. and Focsa, C.: A comprehensive protocol for chemical analysis of flame combustion emissions by secondary ion mass spectrometry, Rapid Commun. Mass Spectrom., 32(13), 1015–1025, doi:10.1002/rcm.8133, 2018.

Irimiea, C., Faccinetto, A., Mercier, X., Ortega, I.-K., Nuns, N., Therssen, E., Desgroux, P. and Focsa, C.: Unveiling trends in soot nucleation and growth: When secondary ion mass spectrometry meets statistical analysis, Carbon N. Y., 144, 815–830, doi:10.1016/J.CARBON.2018.12.015, 2019.

Lohmann, R. and Lammel, G.: Adsorptive and absorptive contributions to the gas-particle partitioning of polycyclic aromatic hydrocarbons: State of knowledge and recommended parametrization for modeling, Environ. Sci. Technol., 38(14), 3793–3803, doi:10.1021/es035337q, 2004.

Marhaba, I., Ferry, D., Laffon, C., Regier, T. Z., Ouf, F.-X. and Parent, P.: Aircraft and MiniCAST soot at the nanoscale, Combust. Flame, 204, 278–289, doi:10.1016/j.combustflame.2019.03.018, 2019.

Moore, R. H., Ziemba, L. D., Dutcher, D., Beyersdorf, A. J., Chan, K., Crumeyrolle, S., Raymond, T. M., Thornhill, K. L., Winstead, E. L. and Anderson, B. E.: Mapping the operation of the miniature combustion aerosol standard (Mini-CAST) soot generator, Aerosol Sci. Technol., 48(5), 467–479, doi:10.1080/02786826.2014.890694, 2014.

Ouf, F. X., Parent, P., Laffon, C., Marhaba, I., Ferry, D., Marcillaud, B., Antonsson, E., Benkoula, S., Liu, X. J., Nicolas, C., Robert, E., Patanen, M., Barreda, F. A., Sublemontier, O., Coppalle, A., Yon, J., Miserque, F., Mostefaoui, T., Regier, T. Z., Mitchell, J. B. A. and Miron, C.: First in-flight synchrotron X-ray absorption and photoemission study of carbon soot nanoparticles, Sci. Rep., 6, doi:10.1038/srep36495, 2016.

Pankow, J. F.: An absorption model of gas/particle partitioning of organic compounds in the atmosphere, Atmos. Environ., 28(2), 185–188, doi:10.1016/1352-2310(94)90093-0, 1994.

Paolini, V., Guerriero, E., Bacaloni, A., Rotatori, M., Benedetti, P. and Mosca, S.: Simultaneous Sampling of Vapor and Particle-Phase Carcinogenic Polycyclic Aromatic Hydrocarbons on Functionalized Glass Fiber Filters, Aerosol Air Qual. Res., 16(1), 175–183, doi:10.4209/aaqr.2015.07.0476, 2017.

Subramanian, R., Khlystov, A. Y., Cabada, J. C. and Robinson, A. L.: Positive and Negative Artifacts in Particulate Organic Carbon Measurements with Denuded and Undenuded Sampler Configurations Special Issue of Aerosol Science and Technology on Findings from the Fine Particulate Matter Supersites Program, Aerosol Sci. Technol., 38(sup1), 27–48, doi:10.1080/02786820390229354, 2004.

Sun, P., Blanchard, P., Brice, K. A. and Hites, R. A.: Trends in Polycyclic Aromatic Hydrocarbon Concentrations in the Great Lakes Atmosphere, Environ. Sci. Technol., 40(20), 6221–6227, doi:10.1021/es0607279, 2006.

Yon, J., Bescond, A. and Ouf, F. X.: A simple semi-empirical model for effective density measurements of fractal aggregates, J. Aerosol Sci., 87, 28–37, doi:10.1016/j.jaerosci.2015.05.003, 2015.

Chemical discrimination of the particulate and gas phases of miniCAST exhausts using a two-filter collection method

Linh Dan Ngo[1,2], Dumitru Duca[1], Yvain Carpentier[1], Jennifer A. Noble[1,*], Raouf Ikhenazene[1], Marin Vojkovic[1], Cornelia Irimiea[3], Ismael K. Ortega[3], Guillaume Lefevre[4], Jérôme Yon[4], Alessandro Faccinetto[2], Eric Therssen[2], Michael Ziskind[1], Bertrand Chazallon[1], Claire Pirim[1], Cristian Focsa[1]

[1]Univ. Lille, CNRS, UMR 8523 – PhLAM – Laboratoire de Physique des Lasers Atomes et Molécules, F-59000 Lille, France
[2]Univ. Lille, CNRS, UMR 8522 – PC2A – Physicochimie des Processus de Combustion et de l'Atmosphère, F-59000 Lille, France
[3]ONERA – The French Aerospace Laboratory, F-91123 Palaiseau, France
[4]Normandie Univ., INSA Rouen, UNIROUEN, CNRS, CORIA, 76000 Rouen, France
[*]now at: CNRS, Aix Marseille Université, PIIM, UMR 7345, 13397 Marseille cedex, France

Correspondence to: Yvain Carpentier (yvain.carpentier@univ-lille.fr)

Abstract. Combustion of hydrocarbons produces both particulate and gas phase emissions responsible for major impacts on atmospheric chemistry and human health. Ascertaining the impact of these emissions, especially on human health, is not straightforward because of our relatively poor knowledge of how chemical compounds are partitioned between the particle and gas phases. Accordingly, we propose to couple a two-filter sampling method with a multi-technique analytical approach to fully characterize the particulate and gas phase compositions of combustion by-products. The two-filter sampling method is designed to retain particulate matter (elemental carbon possibly covered in a surface layer of adsorbed molecules) on a first quartz fiber filter while letting the gas phase pass through, and then trap the most volatile components on a second black carbon-covered filter. All samples thus collected are subsequently subjected to a multi-technique analytical protocol involving two-step laser mass spectrometry (L2MS), secondary ion mass spectrometry (SIMS), and micro-Raman spectroscopy. Using the combination of this two-filter sampling/multi-technique approach in conjunction with advanced statistical methods we are able to unravel distinct surface chemical compositions of aerosols generated with different set points of a miniCAST burner. Specifically, we successfully discriminate samples by their volatile, semi-volatile and non-volatile polycyclic aromatic hydrocarbon (PAH) contents and reveal how subtle changes in combustion parameters affect particle surface chemistry.

1 Introduction

Particulate matter (PM) produced by incomplete combustion of hydrocarbon-based fuels is often found associated to gas phase compounds that include carbon and nitrogen oxides (CO, CO_2, and NO_X), along with a volatile fraction of organic species encompassing low-mass polycyclic aromatic hydrocarbons (PAHs). The presence of PAHs in the atmosphere is of great concern due to their carcinogenic and mutagenic potential (Kim et al., 2013). In fact, in the current European air quality legislation (European Fourth Air quality Daughter Directive 2004/107/EC), seven potentially harmful PAHs must, at least,~~ have to~~ be monitored, but restrictions on PAH concentrations are currently solely limited to benzo[a]pyrene because of its recognized high toxicity (annual target value of 1 ng m^{-3} in the PM10 particulate phase fraction (Pandey et al., 2011)). However, it is the~~a~~ conjunction of the PM intrinsic physico-chemical properties (e.g. nature of adsorbed PAH – Dachs and Eisenreich, 2000 – or water affinity) with pressure, temperature, hygrometric variations or ageing processes in the atmosphere that ultimately condition phase partitioning (free vs bound fraction, Ravindra et al., 2006). Consequently, ~~relatively abundant ~~gas-phase PAHs which are relatively abundant – yet known to bear only weak carcinogenic or mutagenic effects (Nisbet and LaGoy, 1992) – can further react through gas-phase processes or heterogeneous gas-PM exchanges to produce noxious oxy- or nitro-PAHs, for instance (Atkinson and Arey, 1994; Bandowe et al., 2014). PAHs emitted in exhausts, in either the gas phase or the particulate phase, must be analyzed and fully characterized at the same time to better understand their deposition mechanism or chemical transformation in the atmosphere and help ascertain their overall toxicity and impact on human health.

Several methods allowing the concomitant sampling of airborne PAHs in both the gas and particulate phases have been developed in recent~~the last~~ decades (see e.g. the reviews by Pandey et al., 2011; Szulejko et al., 2014; ~~(~~Munyeza et al., 2019~~)~~). The sampling protocol starts with the choice of a suitable sorbent material to either solely capture the vapor phase or solely retain PM. The former sorbent material mostly consists of polyurethane foam, resins, or graphitized carbon black mesh, whereas the latter is~~are rather~~ made of glass fiber, quartz fiber, or Teflon~~ filters~~. The sorbents are placed in series, i.e. one after the other in the exhaust line. The soluble organic fraction is then extracted off-line from the sorbent (filter and/or resin) for subsequent gas chromatography mass spectrometry (GC-MS) analyses (An et al., 2016; Elghawi et al., 2010; Sun et al., 2006). However, such solvent extraction methods exhibit recovery rates that are highly dependent upon the technique applied and the nature of PAHs a priori present. Accordingly, the GC-MS method, which relies on solvent extraction methods and calibration standards, is a time-consuming technique which is inherently more sensitive towards compounds having the greatest solubility. To circumvent this limitation, solvent-free methods have been recently developed based on thermal desorption (e.g. Villanueva et al., 2018), microwave-assisted desorption, or solid-phase micro-extraction (Szulejko et al., 2014). However, because sampling substrates may differ for PM and gas trapping, and often necessitate extraction techniques before characterization whose efficiencies are substrate-dependent, results obtained for the two phases may be difficult to compare and do not necessarily represent the whole PAH family making up either filter.

~~The CAST (Combustion Aerosol Standard) generator is often chosen to produce combustion-generated particles as it is easy to implement for systematic laboratory experiments, the fuel and oxidation air flows being easily modifiable, and hence enables the investigation of a variety of chemistries which can mimic some of the physico-chemical properties of soot particles emitted by real engines (as the ones from aircrafts or cars, e.g. Bescond et al., 2014; Moore et al., 2014).~~ ~~and~~ The CAST (Combustion Aerosol Standard) generator is often chosen to produce combustion-generated particles as it is easy to implement for systematic laboratory experiments with the fuel and oxidation air flows being easily modifiable, and hence enables the investigation of a variety of chemistries. Therefore, using a miniCAST soot generator operated with different parameters as a source of combustion by-products, which can mimic some of the physico-chemical properties of aircraft emissions for instance (Bescond et al., 2014; Marhaba et al., 2019; Moore et al., 2014), allows for potential real-world extrapolations of our results for combustion devices not equipped with after-treatment systems. The proposed method of sampling and characterizing concomitantly the particulate and gas phases can thus be extremely useful when evaluating the impact of various sources (aircraft jet engines, wood combustion stoves, biomass burning) on the environment, as the gas/particulate partitioning conditions the overall reactivity. As it can simultaneously measure the particulate and gas phases, the proposed two-filter method can therefore be utilized to assess the efficiency of after-treatment systems, which are known to successfully remove the majority of particle-bound organic species (Focsa et al., 2019), and more specifically to remove the volatile particles and the organic species from the surface of nonvolatile particles while increasing the contribution of elemental carbon (EC) (Focsa et al., 2019). Time-of-Flight Aerosol Mass Spectrometry (ToF-AMS) has been used in the past by Ferge et al. (2006) and Mueller et al. (2015) to study PAH formation in a~~the~~ CAST generator at different oxidation flows. However, because the samples thus generated are particles, no information about the gas phase composition can be derived in these experiments, which provide only an incomplete picture of the PAH family emitted in the exhausts.

In this work, we coupled a two-filter sampling method with a multi-technique analytical approach to fully characterize the particulate and gas phase compositions of combustion by-products. The two-filter collection method is intended~~s~~ to separate the particulate phase (Front Filter) from the gas phase (Back Filter) using fibrous filtration media (Quartz Fiber Filters – QFF). Once collected, the filters are analyzed using a multi-technique approach encompassing two-step laser mass spectrometry (L2MS), secondary ion mass spectrometry (SIMS), and micro-Raman spectroscopy. The L2MS technique has been extensively developed in our group (at the University of Lille/PhLAM laboratory) over the last decade to specifically probe the chemical composition of combustion byproducts (Delhaye et al., 2017; Faccinetto et al., 2011, 2015; Moldanová et al., 2009; Popovicheva et al., 2017). Its high sensitivity and selectivity towards specific classes of compounds owing to different ionization schemes makes it an extremely valuable analytical tool that can be adapted to various samples. Using three different ionization wavelengths, it is possible to target various classes of compounds such as aromatic and aliphatic compounds. In addition, it is possible to reach a sub-fmol limit of detection for PAHs upon specific desorption and ionization conditions (Faccinetto et al., 2011, 2015). ~~Using three different ionization wavelengths, it is possible to target various classes of compounds and reach sub-fmol limit of detection, e.g. for PAHs (Faccinetto et al., 2011, 2015).~~ The laser desorption process along with its coupling with the subsequent ionization step have been optimized over the years (Faccinetto et al., 2008; Mihesan et al., 2006, 2008) and ensure a soft removal (with minimum internal energy excess) of molecules adsorbed on the particle surface, while avoiding/limiting both their fragmentation and the in-depth damaging of the underlying carbon matrix (Faccinetto et al., 2015). L2MS spectra obtained in this work are additionally reinforced~~backed~~ with the SIMS spectra of deposited miniCAST PM, with no sample preparation prior to the analyses since the particulate matter is preferentially trapped on the Front Filter. Subtle differences and similarities between Front and Back Filters are revealed after mass spectrometry results (L2MS and SIMS) using the recently developed advanced statistical methodologies (Irimiea et al., 2018, 2019) based on principal component analysis (PCA).

2 Experimental methods

2.1 Sample collection

PM was~~ere~~ sampled from the exhausts of a miniCAST generator (5201c) from Jing Ltd., as described previously in e.g. Yon et al. (2018). Briefly, the miniCAST contains a propane-nitrogen flame with operating conditions controlled by the flow rates of propane, nitrogen, oxidation air (Q^{air}) and dilution air. The working points used in this study (and others in this series Bescond et al., 2014; Ouf et al., 2016; Yon et al., 2015) are detailed in Fig. 1. The main difference between these working points is the oxidation air flow and – for the SP4 point – nitrogen dilution, with an increasing oxidation air flow in the order $Q^{\mathrm{air}}_{\mathrm{SP3}} < Q^{\mathrm{air}}_{\mathrm{SP2}} < Q^{\mathrm{air}}_{\mathrm{SP4}} < Q^{\mathrm{air}}_{\mathrm{SP1}}$. Note that the sole dilution system in our experimental setup is that of the miniCAST generator itself (dilution airflow 20 l min^{-1}, Fig. 1). The samples were deposited on quartz fiber filters (QFF, Pall Tissuquartz QAT-UP 2500) using a specially designed sampling line (as illustrated in Fig. 1). A line derivation parallel to the sampling system has been added to ensure the miniCAST is maintained at atmospheric pressure. These QFF are typically used in soot collection, for example in studies of aircraft PM (Delhaye et al., 2017), and are also employed when deriving organic carbon to total carbon (OC/TC) values of deposited soot (Bescond et al., 2016; Yon et al., 2015). QFF are chosen because they proved to be highly efficient in capturing combustion emissions and they have a stable penetration curve among other filters when a range of physical parameters are varying in the sampling line (Zíková et al., 2015). From a theoretical point of view, it is very difficult to predict the collection efficiency of QFF for particles within the nanometer size domain, as generated in our combustion conditions (e.g. 99–166 nm modal diameter, Bescond et al., 2016). Filter collection efficiency is directly related to inertial impaction, direct interception, Brownian diffusion and electrostatic forces (Brochot et al., 2019; Lindsley, 2016; Zíková et al., 2015). The resulting component of these forces is translated into a function that displays near 100 % collection efficiency for particles smaller than 20 nm and larger than 300 nm. The minimum collection efficiency, which is also referred to as the most penetrating particle size (MPPS), is obtained for the 100–300 nm size range. However, some studies showed that the MPPS for QFF may peak around 60 nm and are possibly < 100 nm for other fibrous media (Brochot et al., 2019; Zíková et al., 2015). While these~~is~~ measured values are mostly influenced by both the flow velocity in the sampling line and the pressure drop at the surface of the filter, our flow conditions are close to those used in the work of Zíková et al. (2015). Consequently, we can roughly estimate that the MPPS for the “Front F~~f~~ilter” is below 100 nm. Two filters were used for each sampling period: the “Front Filter” was a bare QFF placed in the exhaust line; the “Back Filter” was a QFF covered with a thin layer of black carbon (Pureblack 100 Carbon, Columbian Chemicals Company, specific surface 80–150 m^2 g^{-1}) and placed 3.5 cm downstream of the Front Filter in the sampling line. Prior to sampling, the Back Filter was heated in an oven at 150°C for 16 hours to remove pre-adsorbed species. Back Filters thus produced were shown to yield no signal when analyzed by L2MS. Black carbon has previously been used as a matrix upon which pure PAHs were adsorbed for mass spectrometric analysis of soot surrogates (Faccinetto et al., 2011, 2015). In the same studies, black carbon-covered filters were also used to sample the volatile fraction in flames. In the present study, the sampling line was designed to collect PM (including adsorbed species) on the Front Filter and to trap gas phase molecules from the remaining exhaust on the Back Filter. Note that particle build-up on the Front Filter could potentially increase its filtration efficiency and consequently trap PAHs that would instead pass through if the thickness of the PM collected on the Front Filter were not as high. Alternatively, species originally adsorbed on the PM can also be desorbed during the sampling and be retained on the Back Filter, which would lead to an overestimation of the gas-phase fraction (Paolini et al., 2017). However, our results will show that if this is the case, only specific PAHs of intermediate volatility are impacted by this phenomenon. In addition, this effect would not affect our statistical analysis (i.e. the covariance between mass peaks (*m/z*)) as similar diffusion behaviors can be expected within SP1 and SP3 samples, which exhibit similar soot porosity (e.g. the porosity of the soot material deposited on silicon wafers for SP1 and SP3 set points were calculated to be about 98.1% and 97.4 %, respectively, Ikhenazene et al., 2019). We therefore expect, from a statistical standpoint, that for each given *m/z*, the covariance will only negligibly be affected by diffusion. Sampling was performed for 20 minutes per working point. ‘Reference’ samples (Front and Back Filters) were collected by running the miniCAST generator for only two minutes under set point SP1 conditions. These samples represent pre-stabilization burner conditions. They were collected as a ‘reference’ to ensure that the samples were not impacted by this early combustion phase, and~~. T~~the loading on these ‘reference’ samples was much lower. After collection, samples were placed in watch glasses covered with Al foil, and stored at 4°C prior to~~before~~ analysis.

2.2 Two-step (desorption / ionization) laser mass spectrometry

Samples were analyzed using a two-step laser mass spectrometry (L2MS) technique built in-house (Mihesan et al., 2008). Briefly, the soot sample is introduced into the analysis chamber (10^{-8} mbar) via a preparation chamber, where it is pre-cooled by a constant flow of liquid nitrogen in the sample holder to avoid the sublimation of the most volatile species. In the analysis chamber of the time-of-flight mass spectrometer (ToF-MS), the sample is irradiated at normal incidence by the beam of a frequency-doubled Nd:YAG laser (Continuum Minilite, λ_d = 532 nm, 4 ns pulsewidth) shaped using a circular aperture and a 10 cm focal length plano-convex CaF_2 lens to form a beam with homogeneous fluence, 0.8 mm-diameter spot on the sample surface. Such irradiation is known to induce the desorption of neutral species from soot without affecting the carbon matrix (Faccinetto et al., 2008). All samples were analyzed with same desorption conditions (λ_d = 532 nm, 400 µJ pulse^{-1}, 80 mJ cm^{-2} i.e. 20 MW cm^{-2}).

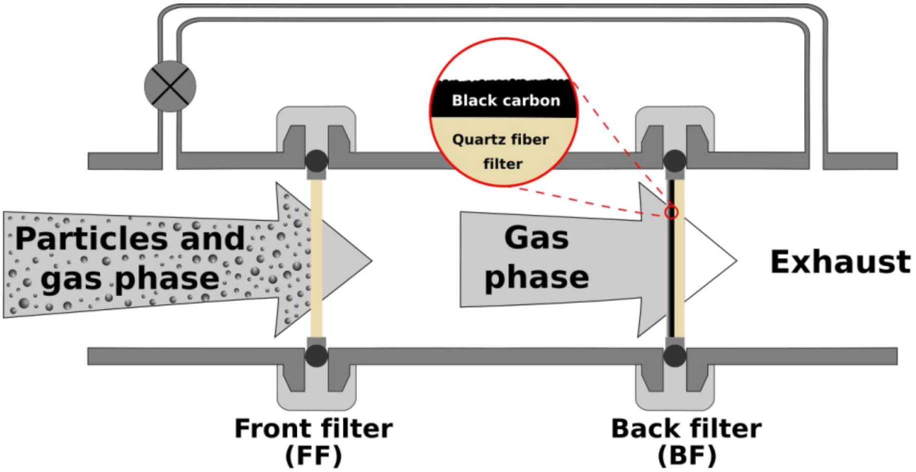

Front Filter	Working point	Fuel (C_3H_8) flow ml min^{-1}	Nitrogen flow ml min^{-1}	Oxidation air flow (Q^{air}) l min^{-1}	Dilution air flow l min^{-1}	Back Filter
	SP1	60	0	1.5	20	
	SP2	60	0	1.15	20	
	SP3	60	0	1.0	20	
	SP4	50	200	1.2	20	

Figure 1. Schematic of the sampling line and photos of sampled soot. The combustion parameters for the miniCAST burner are presented in the table.

The desorbed plume propagates normally from the sample surface towards the extraction plates of the ToF-MS. The molecules from the desorbed plume are then ionized by either a resonant two-photon ionization R2PI (Zimmermann et al., 2001) process at λ_i = 266 nm (4 ns-width pulsed UV laser, Continuum Powerlite, 1 mJ pulse^{-1}) or a single photon ionization (SPI) process at λ_i = 157 nm (5 ns-width pulsed VUV excimer laser, Coherent ExciStar XS 200) or λ_i = 118 nm (in-house built coherent nanosecond source). The ninth harmonic of the Nd:YAG laser (λ_i = 118.2 nm) was generated by tripling the 355 nm output of a Continuum Surelite pulsed laser in a Xe cell (Hilbig, 1982; Popovicheva et al., 2017). For the two SPI wavelengths, the setup was optimized to the maximum output (i.e. maximum electric potential for the 157 nm excimer laser, and maximum pumping energy for the 355 nm laser (34 mJ pulse^{-1}) to maximize 118 nm conversion, at an estimated conversion efficiency of 0.01 % (Butcher, 1999). The time delay between desorption and ionization is set to 100 µs by a digital delay/pulse generator (Stanford DG535). Generated ions are then mass analyzed in a 1.72 m-long reflectron ToF-MS (RM Jordan) with a mass resolution of *m/Δm* 1000. Ion detector signals are recorded using a digital oscilloscope (LeCroy Waverunner 9350AM) at a time resolution of 4 ns/point. Each spectrum corresponds to an average of at least 200 desorption shots at different locations on the sample. A set of ~~5~~ 3 spectra was obtained for each miniCAST sample (FF and BF) and each ionization scheme. Therefore, in total, 18~~30~~ spectra were obtained for each miniCAST set point.

2.3 Secondary ion mass spectrometry

Time-of-Flight Secondary Ion Mass Spectrometry analysis was conducted with TOF.SIMS^5 instrument from ION-TOF GmbH. Briefly, samples were introduced into the analysis chamber with a residual pressure of 10^{-8} mbar. The sample surface was bombarded by a 25 keV Bi_3^+ ion beam with a current of 0.3 pA in static mode. A 180 s acquisition time and 25 random scans/acquisition were used for an analyzed area of 500 µm × 500 µm on the sample surfaces. Mass spectra were collected in both positive and negative polarities for at least three areas per sample. The mass resolution at *m/z* 29 is approximately 2700. For this analysis samples are not cooled down. Ion signals in SIMS mass spectra were identified and calibrated using SurfaceLab 6 software from ION-TOF GmbH. Positive spectra were calibrated with peaks C^+ (*m/z* 12.000), CH_3^+ (*m/z* 15.023), $C_7H_7^+$ (*m/z* 91.055), $C_{16}H_{10}^+$ (*m/z* 202.078), and $C_{19}H_{11}^+$ (*m/z* 239.086). Negative spectra were calibrated with peaks at C^- (*m/z* 12.000), CH^- (*m/z* 13.008), O^- (*m/z* 15.995), C_2^- (*m/z* 24.000), C_4H^- (*m/z* 49.008), and C_8H^- (*m/z* 97.008). A set of 5 spectra was obtained for each miniCAST sample (FF and BF) and each polarity. Therefore, in total, 20 spectra were acquired for each miniCAST set point.

2.4 Raman micro-spectroscopy

Raman analyses were performed with an Invia reflex spectrometer (Renishaw) equipped with an Olympus microscope (BXFM) (Chazallon et al., 2014). The spectra presented in this work were obtained by irradiation with a 514 nm laser with a nominal power of 150 mW. The laser power was reduced to avoid thermal effects at the sample surface. Using a lens with 20× magnification (N.A. 0.5), the laser was focused on the sample surface with a spot of 3.0 µm diameter. The spectrometer was calibrated using the Stokes Raman signal of pure Si at 520 cm^{-1}. Raman spectra of spectral resolution 12 cm^{-1} were collected at four different spots on each sample using integration times of 60 s with 10–20 scans accumulated per spectrum.

2.5 Multivariate data analysis: principal component analysis (PCA)

PCA is a technique used to highlight variation and patterns in a data set, and in this case was used to reveal the differences in chemical composition of the samples, and in particular between (i) Front and Back Filters and (ii) miniCAST set points. PCA is very convenient to outline the subtle differences between data sets, since it reduces the dimensionality of complex data while preserving most of the information. PCA was applied to each of the five datasets (3 L2MS ionization wavelengths and 2 SIMS polarities) following the procedure detailed in Popovicheva et al. (2017), Irimiea et al. (2018), and Duca et al. (2019). Further information can also be found in Sect. S2. Briefly, each mass spectrum was represented by a set of values corresponding to the integrated area of a selected number of mass peaks in the spectrum. The number of selected mass peaks was 66, 105, and 60 in L2MS mass spectra recorded at λ_i = 266, 157, and 118 nm, respectively, and 138 and 70 in SIMS mass spectra recorded in positive and negative polarity, respectively. PCA analyses were performed using a covariance matrix, i.e. each data set was organized into a matrix containing observations/samples (arranged in rows) and variables/peak integrated area (arranged in columns). Principal components (PCs) were constructed as linear combinations or mixtures of the initial variables (peak integrated areas). The physical meaning of all derived PCs can be inferred from the contribution of the various molecular species to the loadings, i.e. by determining the relative importance of each mass peak integrated area to the main variance in the data set. Scree plots and loadings for all L2MS PCA analyses discussed in this article can be found in the supplementary material (Fig. S2 and S3). It should be further noted that initial PCA tests included 'reference' samples (in both L2MS and SIMS PCAs). This preliminary step resulted in PC1 (the largest variance in the data set) being dominated by the variance between the 'reference' samples (Front and Back Filters) and all other samples, confirming that the early pre-stabilization deposition does not influence the spectra of the various set points measured. After this confirmation step, the 'reference' samples were removed from the covariance matrix used to perform the PCA and therefore are not presented in the following sections.

3 Results and Discussion

3.1 L2MS analysis

3.1.1 Mass spectra obtained by L2MS at individual ionization wavelengths

L2MS mass spectra of samples SP1, SP2, SP3, and SP4 (for both Front and Back Filters) produced at three different ionization wavelengths (266, 157, and 118 nm) are discussed in this section. Mass spectra obtained with a 266 nm ionization wavelength are presented in Fig. 2, whereas results obtained for 157 and 118 nm are both presented in Fig. S1.

Upon 266 nm ionization, all mass spectra are dominated by signals attributed to aromatic species, and more specifically to PAHs (Fig. 2). An important advantage of L2MS is to generate, for the most part, fragment-free mass spectra while maintaining a high signal-to-noise ratio, due to the controlled desorption and ionization fluences (Faccinetto et al., 2011). On all mass spectra generated with a 266 nm ionization wavelength, the lightest detected PAH is naphthalene ($C_{10}H_8^+$, *m/z* 128). On Front Filters (λ_i = 266 nm, Fig. 2), the heaviest detected mass varies from sample to sample: $SP1_{FF}$ – *m/z* 400, $SP2_{FF}$ – *m/z* 546, $SP3_{FF}$ – *m/z* 546, and $SP4_{FF}$ – *m/z* 522. The base peak is at *m/z* 202 for $SP2_{FF}$, $SP3_{FF}$, and $SP4_{FF}$, and at *m/z* 178 for $SP1_{FF}$. One can observe that the increase in oxidation air flow ($Q^{air}_{SP3} < Q^{air}_{SP2} < Q^{air}_{SP4} < Q^{air}_{SP1}$) results in a significant variation in the shape of the mass spectra. In the SP1 regime, most of the signal comes from three- and four-ring PAHs, while the heavier PAHs are less conspicuous. Regimes with~~having~~ the lowest oxidation air flow tend to produce more of the heavier PAHs, although the increase in~~of~~ contribution for each mass is not the same. For samples $SP2_{FF}$ and $SP4_{FF}$ most of the PAHs are concentrated in the mass range *m/z* 178–350 ($C_{14}H_{10}^+$–$C_{28}H_{14}^+$), with comparable relative intensities. However, the SP3 regime has high peak intensities for $C_{14}H_{10}^+$ (*m/z* 178), $C_{16}H_{10}^+$ (*m/z* 202), $C_{18}H_{12}^+$ (*m/z* 228), and $C_{20}H_{12}^+$ (*m/z* 252), while the relative contributions of heavier PAHs remain comparable. Literature data converge towards the fact that the SP3 set point is distinct from the others in that i) the organic to total carbon ratio is higher (87% versus ≤ 47% for the other set points), and ii) the crystallites of the particles produced in these conditions are significantly smaller and form a distinct disordered arrangement exhibiting many carbon edges (Bescond et al., 2016; Marhaba et al., 2019; Ouf et al., 2016; Yon et al., 2015). Such smaller crystallites suggest that SP3 may undergo nucleation and growth processes different from those of the other set points, subsequently leading to distinct chemical compositions (e.g. different isomeric distributions) of the PM. The relative ion signals observed between the Front and Back Filters hence depend upon the relative volatilities and the response of the chemical compounds present on the samples to the 266 nm R2PI L2MS.

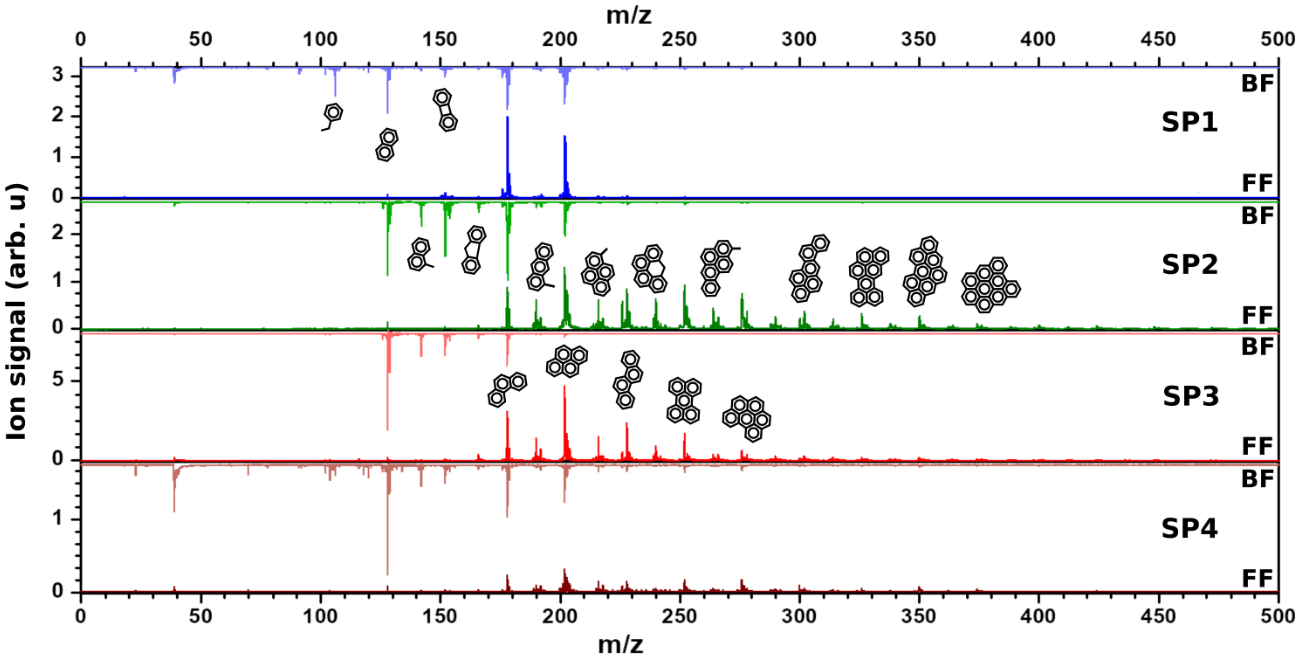

Figure 2. Comparison between mass spectra for SP1, SP2, SP3, and SP4 samples recorded with λ_i = 266 nm for Front Filters (lower spectra) and Back Filters (upper spectra). Note that four different areas have been averaged to yield each of these spectra. Proposed structural formulae based on molecular formulae~~s~~ obtained from mass spectra are also shown.

On Back Filters (λ_i = 266 nm, Fig. 2), the signal is mostly concentrated in a lower mass region than that of Front Filters. Mass spectra of all Back Filters are dominated by *m/z* 128 (naphthalene, $C_{10}H_8$). The spectrum of $SP4_{BF}$ shows more peaks of higher masses than what is observed on other samples. The first aromatic compound visible on all samples is benzene (*m/z* 78), however its intensity is drastically reduced for both $SP2_{BF}$ and $SP3_{BF}$ compared to that of $SP1_{BF}$ or $SP4_{BF}$. The same trend is observed for aromatic compounds lighter than *m/z* 128. Oxidation air flows associated with set points SP4 and SP1 thus resulted in the formation of more of the smallest-sized aromatic species (*m/z* 78–128).

-The various miniCAST set points exhibit different PAH mass distributions on their Front and Back Filters, which likely relates to the different volatility properties of PAHs and probably affects their subsequent trapping on Front and Back Filters.

Distinct volatility properties have been observed in the past on particles originating from wood combustion by Bari et al. (2010), who classified the PAHs on the basis of their number of aromatic rings resulting in the detection of three different PAHs categories. The authors classified the PAHs consisting of two aromatic rings as volatiles as they were mostly found in the gas phase, while those made of three and four rings were classified as semi-volatiles. PAHs comprising more than four rings were classified as non-volatile as they were observed in the PM in their study. Note that slightly different classes have also been defined elsewhere in the literature (An et al., 2016; Elghawi et al., 2010; Sun et al., 2006). In our study, we largely found compounds consisting of one and two aromatic rings on Back Filters, while PAHs of *m/z* 176–242 were found on both Back and Front Filters and those of *m/z* ≥ 252 predominantly on Front Filters. Such PAH partitioning between Front and Back Filters is in line with the work of Bari et al. (2010). Similarly, we categorized the PAH distributions found on miniCAST samples into a volatile, semi-volatile, and non-volatile fraction (Fig. 3), where the volatile fraction here encompasses aromatic species made of one to two aromatic rings (*m/z* 78–166), the semi-volatile fraction comprises PAHs with a mass range of *m/z* 176–242, and the non-volatile fraction includes PAHs of *m/z* ≥ 252. The boundaries of these intervals have been refined using the representation of Fig. 3 in which the “contrast function” defined as the $\frac{S_{FF}-S_{BF}}{S_{FF}+S_{BF}}$ ratio is represented for the 266 nm L2MS data, where S_{FF} and S_{BF} are the ion signals associated with a mass peak on the Front Filter and the Back Filter, respectively. This representation clearly underlines that small aromatic species are found solely on the Back Filters, whereas large PAHs are mostly on the Front Filters.

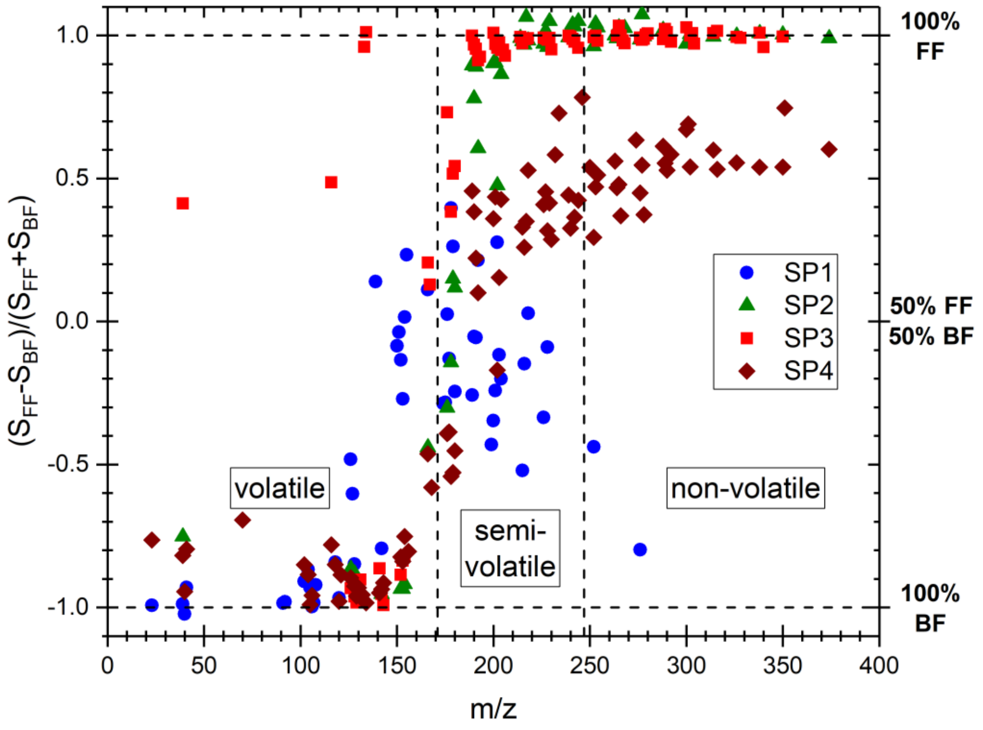

Figure 3. "Contrast plot" representing the variation in PAH signal detected with L2MS at λ_i = 266 nm for the four miniCAST set points. Values on the y-axis correspond to the partitioning of the species between the Front Filters and Back Filters: -1 indicates that the species are all found on the BF, +1 that they are all found on the FF, and 0 that they are equally partitioned on both filters.

The total PAH signal derived from L2MS measurements (λ_i = 266 nm) can be further refined according to the PAH mass range distribution present on each sample (Fig. 4) as previously defined in Fig. 3. Delhaye and coworkers showed that the total PAH signal in mass spectra obtained with λ_i = 266 nm can be indicative of the presence of organic carbon in aeronautical soot samples, because of the good agreement between total PAH mass signal and OC/TC values derived by a commonly ~~-~~used thermo-optical protocol (see Fig. 7 in Delhaye et al., 2017). In Fig. 4~~3~~, the total PAH signal, corresponding to the sum of all peaks attributed to PAHs in the 266 nm normalized mass spectra, is plotted against the oxidation air flow and is further compared to the OC/TC values given in Bescond et al. (2016) and Yon et al. (2015). According to these studies, SP1 has the lowest OC/TC ratio at 4.1 %, followed by SP4 (OC/TC 22.1 %), SP2 (OC/TC 46.8 %), and SP3 (OC/TC 87 %). Slightly different values for SP2 (OC/TC 58.3 %) and SP1 (OC/TC 16.2 %) are given by Yon et al. (2015), but the same overall trend is maintained. The same evolution with oxidation air flow was evidenced for the PAH to soot ratio in Moore et al. (2014) using a different method (photoelectric aerosol sensor). Figure 4~~3~~ shows that the total PAH signal measured by mass spectrometry (λ_i = 266 nm) on Front Filters (orange bars) follows the same trend as the OC/TC ratios measured by the thermo-optical protocol for the same miniCAST set points (Bescond et al., 2016; Yon et al., 2015). Although the total PAH signal on Back Filters (blue bars, Fig. 3) also follows the trend observed on Front Filters for samples $SP3_{BF}$, $SP2_{BF}$, and $SP4_{BF}$ (decreasing PAH signal with increasing oxidation air flow), total PAH signal of $SP1_{BF}$ is high compared to that of $SP1_{FF}$. This is likely due to the nature of its PAH content for this set point, which likely includes more volatile and semi-volatile aromatic species ~~as discussed later on~~.

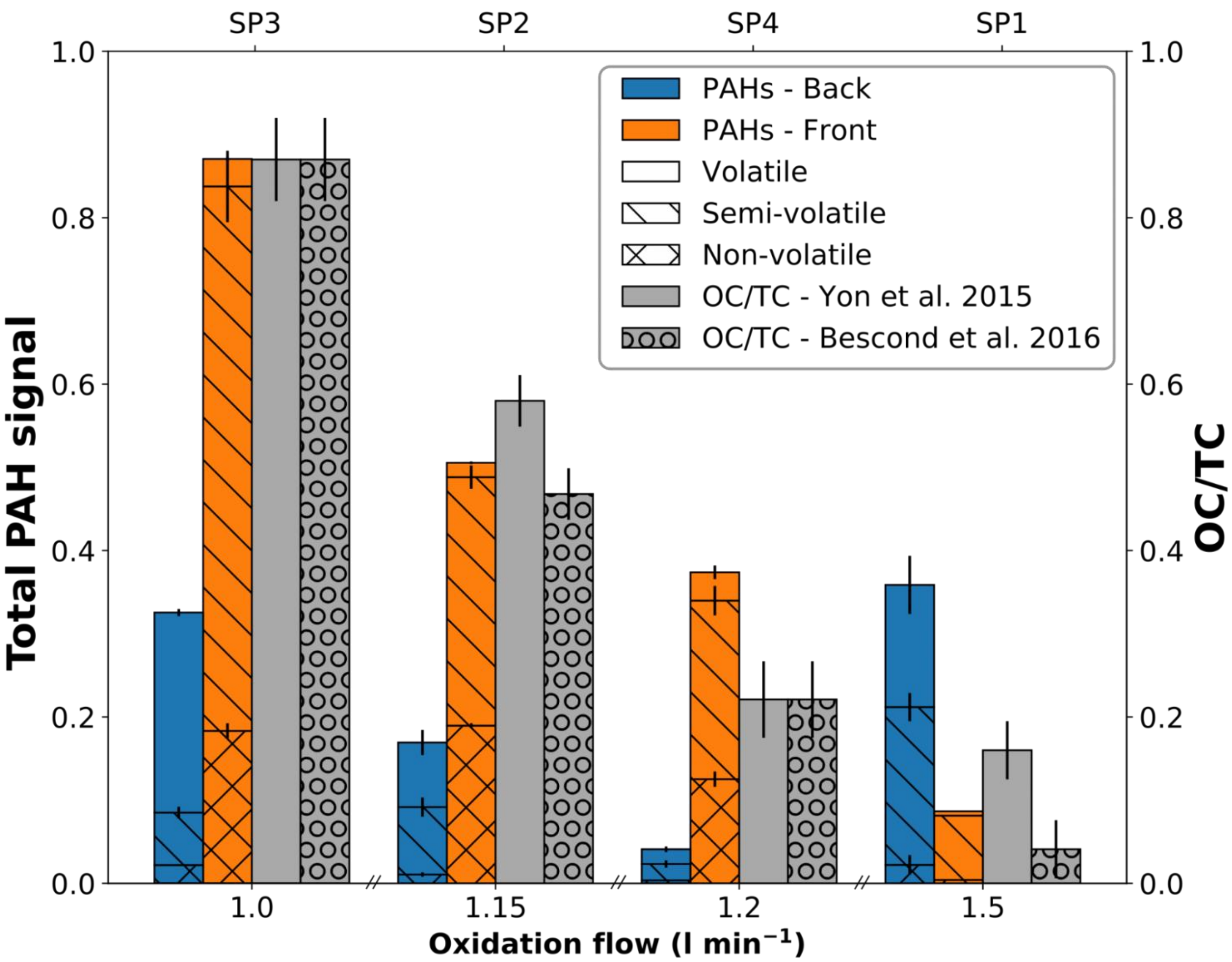

Figure 4. Variation in total PAH signal detected with L2MS at λ_i = 266 nm on Front (orange) and Back (blue) Filters plotted as a function of oxidation air flow. The PAH contribution is divided into adsorbed species (non-volatile, *m/z* ≥ 252), semi-volatile (*m/z* 176–242), and volatile (*m/z* 78–166) fractions. OC/TC values reported in the literature are plotted in grey for comparison.

In order to access other classes of molecules, the miniCAST set points have been also analyzed using 157 and 118 nm ionization wavelengths. The majority of PAHs were also detected with SPI at 157 nm for both Front and Back Filters, albeit at a lower signal intensity (as can be seen by comparing the two sets of spectra in Fig. 2 and Fig. S1). The overall shape changes due to the different ionization efficiencies of PAHs from R2PI at 266 nm and~~to~~ SPI at 157 nm. At lower masses, additional peaks with prominent features at *m/z* 28, 43, 55, 69 are present and are assigned to aliphatic fragment ions, which could result from multi-photon ionization processes. Analysis of the peak at *m/z* 31 suggests the presence of heteroatoms in the fragments as it cannot be assigned to a $C_nH_m^+$ hydrocarbon formula. The series *m/z* 91, 103, 115 corresponds to fragments ($C_7H_7^+$, $C_8H_7^+$, $C_9H_7^+$), which are attributed to alkylbenzene species (McLafferty and Tureček, 1993).

Mass spectra obtained with SPI at 118 nm (Fig. S1) show a high degree of fragmentation. In all cases, peaks at *m/z* 23 and 39 are due to the presence of trace amounts of usual contaminants Na and K. PAHs were detected on all samples, but the signal intensity is low due to a high fragmentation rate caused by the excess of energy at λ_i = 118 nm. Fragment ions at *m/z* 50, 51, 52, 53, 63, and 65 suggest also the presence of aromatic compounds. Series of highly unsaturated aliphatic compounds ($C_{2n}H_2^+$ and $C_{2n}H_4^+$, n = 2–5) are present. Fragments of alkyl compounds ($C_nH_{2n+1}^+$) were also found at *m/z* 15, 29, 43, 57, 71, 85, and 99, with a relatively low intensity compared to fragments of aromatic compounds. Another distinctive series – attributed to $C_nH_{2n}^+$ fragments – was found at *m/z* 28, 42, 56, and 70. These fragments may result from a McLafferty rearrangement involving alkene chains (McLafferty and Tureček, 1993).

In conclusion, our L2MS results for the three ionization wavelengths converge to show that heavy PAHs (*m/z* ≥ 252) are largely found on the Front Filters, whereas the volatile aromatic species (1–2 rings) are solely detected on the Back Filters. This detailed mass spectrometry analysis following our two-filter collection system shows very effective partitioning of the PM/gas phases on FF and BF and a clear dependence on the volatility of the molecules. We find that the total PAH content varies with the oxidative air flow, as shown in previous studies. Finally, this two-filter system allows us to evidence subtle differences in the chemical composition of the various miniCAST set points.

3.1.2 Principal component analysis of L2MS spectra

In order to better discriminate the chemical composition of the various samples, particularly (i) the Front and Back Filters and (ii) the miniCAST set points, principal component analysis (PCA) was applied to mass spectra recorded for all three individual ionization wavelengths. A full description of this statistical method is provided in Sect. S2. Here, the covariance matrix was built from the integrated areas of all the detected peaks with a signal-to-noise ratio SNR > 3. The physical meaning of all derived principal components can be inferred from the contribution of the various molecular species to the loadings (see Sect. S2 and Fig. 5b~~S2~~ and S3). By identifying the molecular families contributing to this variance, we can ~~better~~ interpret the PCA score plots (Fig. 5~~4~~) and grasp the nature of the subtle chemical differences between the samples.

In L2MS data generated with 266 nm ionization wavelength, the scree ~~plot~~ and loading~~s~~ plots presented in Fig. 5b~~S2a~~ and S2a~~S3a~~, respectively, show that PC1 expresses the largest variance (58.86 %) in the dataset and differentiates samples represented by a greater amount of high-mass PAHs (positive contribution: *m/z* ≥ 189) from those containing more of low-mass aromatic species~~PAHs and derivatives~~ (negative contribution: up to three aromatic rings), especially naphthalene (*m/z* 128). PC2 (19.30 %) denotes the relative contribution between high-mass PAHs (positive contribution: *m/z* ≥ 216) bearing four and more aromatic rings and aromatic compounds containing up to *m/z* 202, especially m/z 178 and 202, and benzene and its alkyl-derivatives~~the mass of pyrene (*m/z* 202)~~. The dataset, in terms of PC1 and PC2, is illustrated in a score plot in Fig. 5~~4~~a. ~~There is a notable separation between different samples which implies distinct chemical compositions of PM on the filters. The first conclusion is that, for all set points, PC1 is positive for Front Filters but negative for Back Filters, and~~

~~therefore the main difference between Front and Back Filters can be defined as the greater amount of high-mass PAHs (*m/z* ≥ 189) on Front Filters. The highest PC1 score is observed for SP2$_{FF}$, therefore it has the highest relative contribution from the high-mass PAHs, while SP3$_{BF}$ (the most negative score of PC1) contains mostly light-weight aromatic species (≤ 3 aromatic rings). The PC1 score for Back Filters decreases along with the oxidation air flow indicating a greater contribution of aromatic species with 3 or less aromatic rings for lower oxidation air flows. Data points for Front Filters generally display a positive PC2 component except for SP1$_{FF}$, a phenomenon possibly explained by the small fraction of non-volatile PAHs produced in this regime.~~According to PC1, the largest separation appears between sample groups SP2–4$_{FF}$ and SP1–4$_{BF}$. It can be attributed to the higher fraction of high-mass PAHs (*m/z* ≥ 189) relative to smaller aromatic species for the former group compared to the latter. The first conclusion is that our samples are mainly separated regarding their chemical composition (non-volatile and semi-volatile fractions vs volatile fraction) because of the two-filter collection system rather than the miniCAST operating conditions. However, a refined observation in the PCs can help to interpret composition variations between the different set points. For Back Filters, the PC1 score decreases along with the oxidation air flow indicating a greater contribution of small aromatic species, especially naphthalene, for lower oxidation air flows. Data points for Front Filters generally display a positive PC2 component except for SP1$_{FF}$, a phenomenon possibly explained by the very small fraction of non-volatile PAHs produced in this regime relative to *m/z* 178 and 202. The almost constant score of PC2 for SP2–4$_{FF}$, which is in contrast with the very different scores for the Back Filters (Fig. 5a), and the high contribution of semi-volatile species to the PC2 loadings (Fig. 5b) highlights that the ratios of semi-volatile compounds vary between the Front and Back Filters for the different set points. This observation demonstrates that the partitioning between the Front and Back Filters is not only driven by thermodynamic conditions (volatility) but also by the nature of the soot matrix produced at the different set points. Note that details about the PCA applied to the 157 nm and 118 nm L2MS data can be found in the supplementary material. The statistical approach developed in this section confirms from a quantitative standpoint the descriptive results obtained in Sect. 3.1.1.

~~In L2MS data generated with a 157 nm ionization wavelength, the scree plot and loadings displayed in Fig. S2b and S3b, respectively, show that PC1 (55.38 %) can be interpreted as the relative contribution of semi- and non-volatile PAHs and fragments (positive contribution) to fragments at *m/z* 25 and 26 and the very few volatile aromatic species (*m/z* 104, 128, 142, 152, 154, and 178, negative contribution), whereas PC2 (20.55 %) exhibits a positive contribution solely from semi-volatile species (*m/z* 176–242). Fig. 4b shows no clear separation between Front and Back Filters at this ionization wavelength. This is expected as the ionization energy (157 nm, 7.9 eV) is not enough to ionize naphthalene or its methyl derivatives, representative of the volatile compounds expected to be present in the gas phase (Bari et al., 2010). However, SP2$_{FF}$ once again exhibits the highest PC1 score, meaning that its mass spectrum contains a large amount of semi- and non-volatile species. SP3$_{FF}$ displays the highest PC2 score which translates into a high contribution from semi-volatile compounds. Low oxidation air flow conditions (SP3) result in the production of more semi-volatile compounds, while SP2 conditions generate a higher relative contribution from non-volatile compounds, resulting in more homogeneous mass~~

~~spectra. While this ionization wavelength did not provide information on lightweight or volatile organic compounds, it yet confirmed the separation between semi and non-volatile compounds with CAST set points.~~

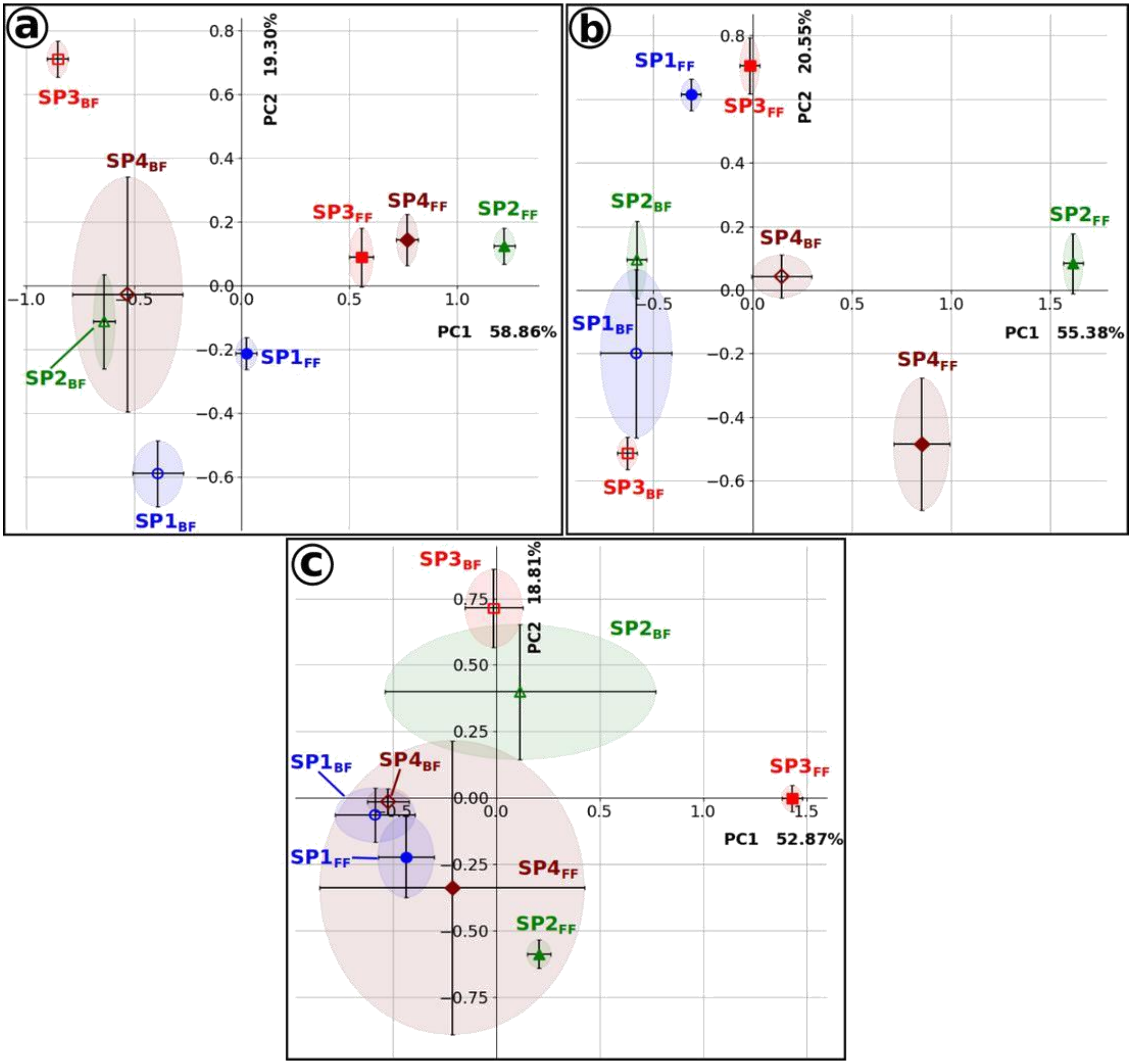

~~**Figure 4.** Score plots of PC2 vs PC1 derived from principal component analysis of the data obtained with 266 nm (a), 157 nm (b), and 118 nm (c) ionization.~~

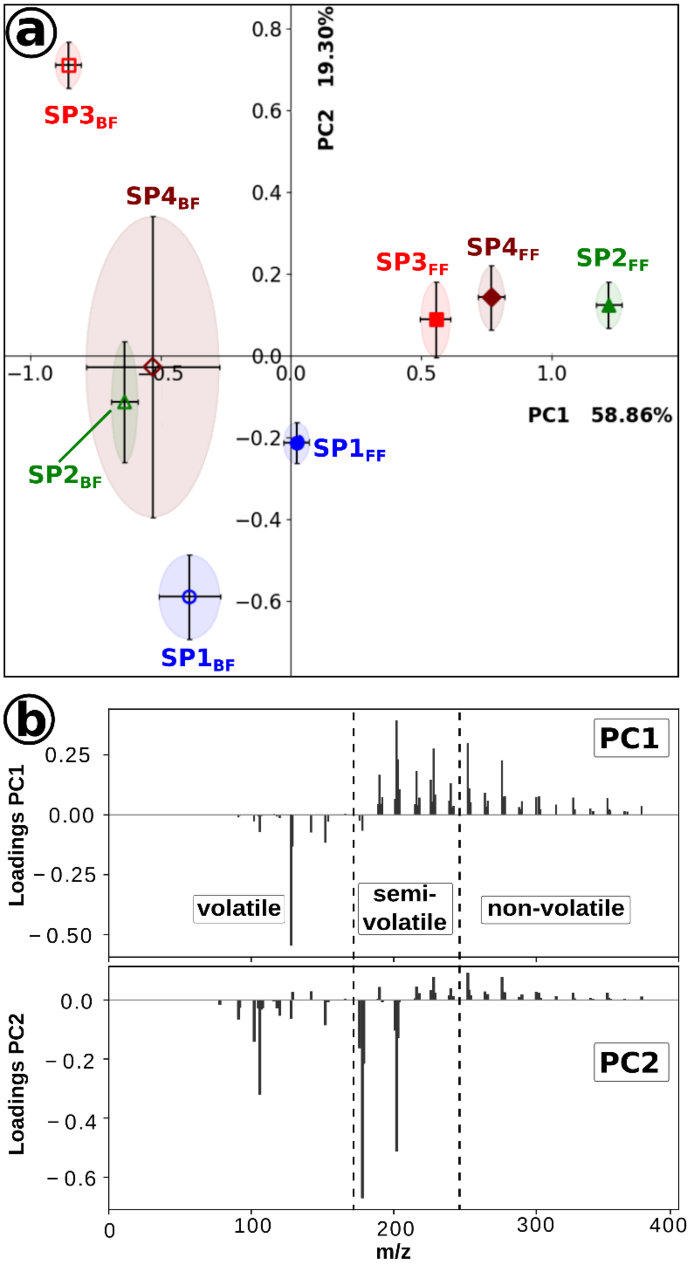

Figure 5. Score (a) and loading (b) plots of PC2 and PC1 derived from principal component analysis of the L2MS data obtained with 266 nm ionization.

~~In L2MS data generated with 118 nm ionization wavelength, the scree plot and loadings displayed in Fig. S2c and S3c, respectively, show that PC1 represents the contribution from aromatic compounds (*m/z* 178–252), while lower masses (*m/z* 50–98) largely influence PC2, and in particular $C_{2n}H_2^+$ and $C_{2n}H_4^+$. $SP3_{FF}$ is the only sample with a relatively high contribution of aromatic compounds compared to low masses, resulting in a large PC1 score as seen in Fig. 4c. All other samples show a relatively low amount of aromatic species, and hence they do not diverge significantly in terms of PC1. Nevertheless, there is a clear trend in the aromatic contribution (AC), which increases ($AC_{SP1} < AC_{SP4} < AC_{SP2} < AC_{SP3}$) as the oxidation air flow decreases. $SP2_{FF}$ contains the most $C_{2n}H_2^+$ and $C_{2n}H_4^+$, followed by $SP4_{FF}$. For the SP2 and SP3 regimes, it appears that $C_{2n}H_2^+$ and $C_{2n}H_4^+$ are mostly found on the PM, while for other working points the difference between their concentrations on Front and Back Filters is minimal.~~

3.2 SIMS analysis

3.2.1 Mass spectra obtained by SIMS

SIMS measurements are complementary to L2MS analysis as they can provide insights into the compounds that preferentially produces negative ions. For the sake of comparison with L2MS results, SIMS measurements were first obtained in positive mode. Positive ~~S~~spectra of SP1, SP2, SP3, and SP4 samples ~~obtained with ToF-SIMS in positive mode~~ are presented in Fig. ~~5~~ 6 (*m/z* 150–500 range). All SIMS mass spectra feature ~~a~~ significant fragmentation, which is intrinsic to the technique and caused by the energetic primary ion beam. To start with Front Filter samples, and similarly to what has been observed in L2MS, the PAH distribution across samples varies with set points, the highest detected mass on $SP1_{FF}$, $SP2_{FF}$, $SP3_{FF}$, and $SP4_{FF}$ being *m/z* 452, *m/z* 871, *m/z* 825, and *m/z* 908, respectively. ~~Again,~~ $SP1_{FF}$ shows a shorter high-mass PAH "tail" compared to other Front Filter samples. The high-mass PAH region observed in SIMS is in good agreement with that of L2MS, whereas the significant fragmentation observed in SIMS seems to impair the low-mass region (ca. $m/z < 228$) more conspicuously and as a result makes SIMS and L2MS spectra look more distinct in this region. It is worth recalling ~~also~~ that SIMS measurements are performed at room temperature, which contrasts with L2MS measurements that involve nitrogen cooling. This may potentially~~eventually~~ result in SIMS analyses providing an incomplete picture for some specific low-mass PAHs~~ (especially the volatile PM fraction), as further discussed below~~. The base peak of $SP2_{FF}$, $SP3_{FF}$, and $SP4_{FF}$ samples is located at *m/z* 239 ($C_{19}H_{11}^+$), whereas $SP1_{FF}$ exhibits its highest intensity peak at *m/z* 202 ($C_{16}H_{10}^+$). The absolute intensity of the overall signal is the highest for $SP3_{FF}$, followed by $SP2_{FF}$, $SP4_{FF}$, and $SP1_{FF}$. Likewise, the total PAH contribution in each sample (i.e. summed areas of all peaks attributed to PAHs in positive mode) decreases with the oxidation air flow rate for Front Filters, as shown in Fig. 7~~6~~, which indicates that the general trend previously shown with L2MS is also observed with SIMS. Consequently, the total PAH signal derived from SIMS measurement is also in line with OC/TC measurements obtained from thermo-optical methods (Bescond et al., 2016; Yon et al., 2015) for all Front Filter samples (Fig. 7~~6~~). Here, non-volatile species are predominant on $SP3_{FF}$, $SP2_{FF}$, and $SP4_{FF}$, while semi-volatiles constitute the main class of compounds observed on SP1$_{FF}$. The~~ difference in which~~ prevalent class of chemical compounds ~~is predominant~~ in L2MS or~~and~~ SIMS mass spectra (Fig. 4~~3~~ vs Fig. 7~~6~~) is linked~~due~~ to the ionization process (λ_i = 266 nm vs Bi_3^+ ion beam). Semi-volatile compounds (*m/z* 178–228) are prevalent~~dominant~~ in spectra generated with 266 nm ionization wavelength, whereas high-mass aromatic compounds (*m/z* 250–500) dominate SIMS mass spectra. This suggests that miniCAST samples contain PAHs with a high stability in the high-mass range (i.e. stabilomers, Stein and Fahr, 1985), which are eventually less prone to fragmentation in SIMS with respect to other semi-volatile compounds. Consequently, a smaller relative fraction of molecules is fragmented in L2MS which leads to a more reliable PAH content determination in the semi-volatile mass range from their L2MS mass spectra compared to SIMS.

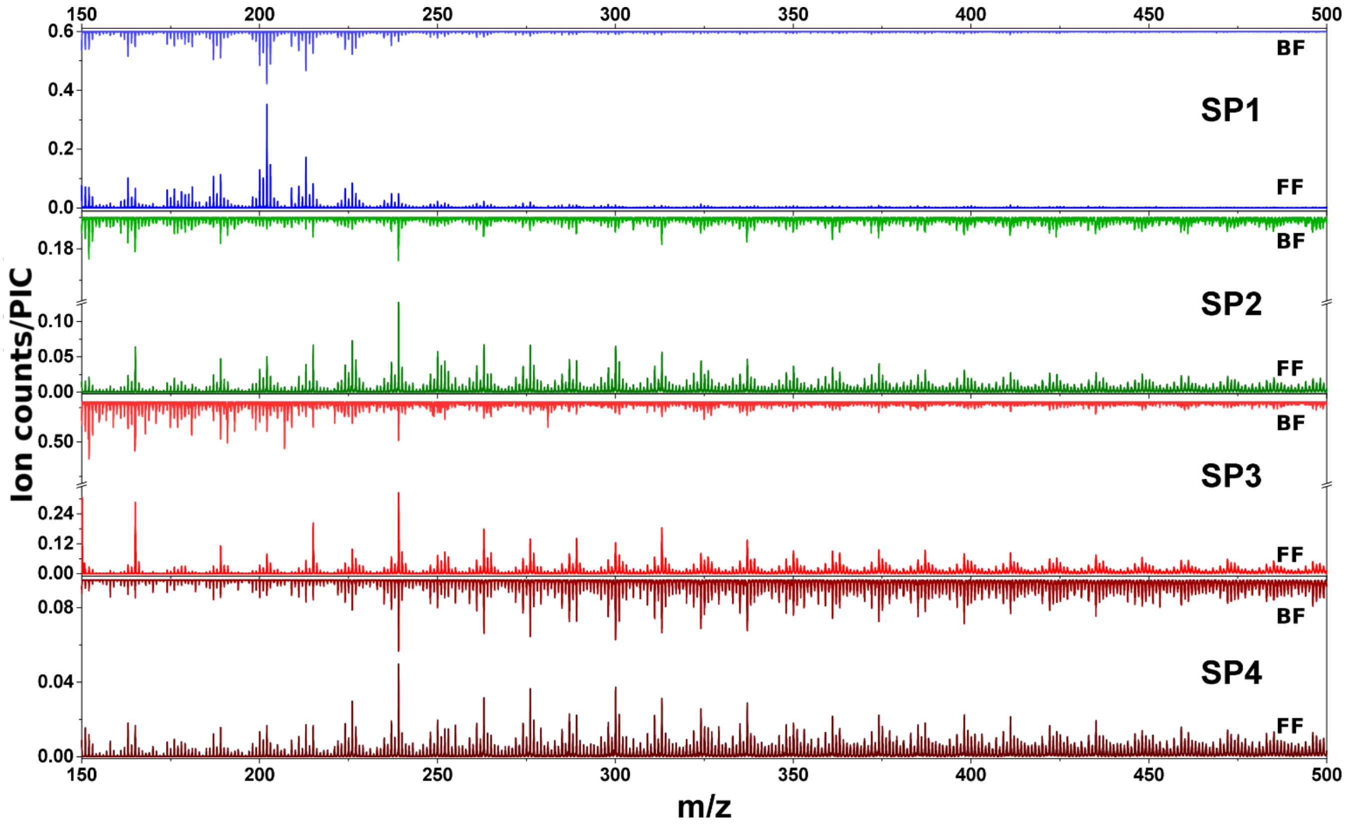

Figure 6~~5~~. ToF-SIMS mass spectra of samples SP1, SP2, SP3, and SP4 obtained in positive polarity for Front Filters (lower spectra) and Back Filters (upper spectra). For visualization purposes, we focus on the *m/z* 150–500 range. Note that for SP2 and SP3 samples Front and Back filters have different scales.

As to the PAH distribution observed on Back Filters, it is distinct from that of Front Filters in that the highest mass detected is *m/z* 411 on SP1$_{BF}$, *m/z* 570 on SP2$_{BF}$, *m/z* 448 on SP3$_{BF}$, and *m/z* 793 on SP4$_{BF}$ (i.e. the *m/z* distribution of Back Filters is less spread out towards high masses). The total PAH signal shows now a different behavior to that observed on Front Filters

(Fig. 7~~6~~), where SP4$_{BF}$ exhibits the highest PAH signal, followed by SP2$_{BF}$, SP1$_{BF}$, and SP3$_{BF}$. Additionally, the PAH signal of SP4$_{BF}$ determined by SIMS is higher than the one of its corresponding Front Filter, which is in contradiction to what has been derived from L2MS (λ_i = 266 nm) spectra, where the Front Filter showed a much higher PAH signal. This behavior may originate from the nature of deposited PAH on Front and Back Filters, which may have different volatility and stability properties and hence will react differently to the energetic Bi_3^+ ion beam used in SIMS analysis.~~, as discussed above.~~

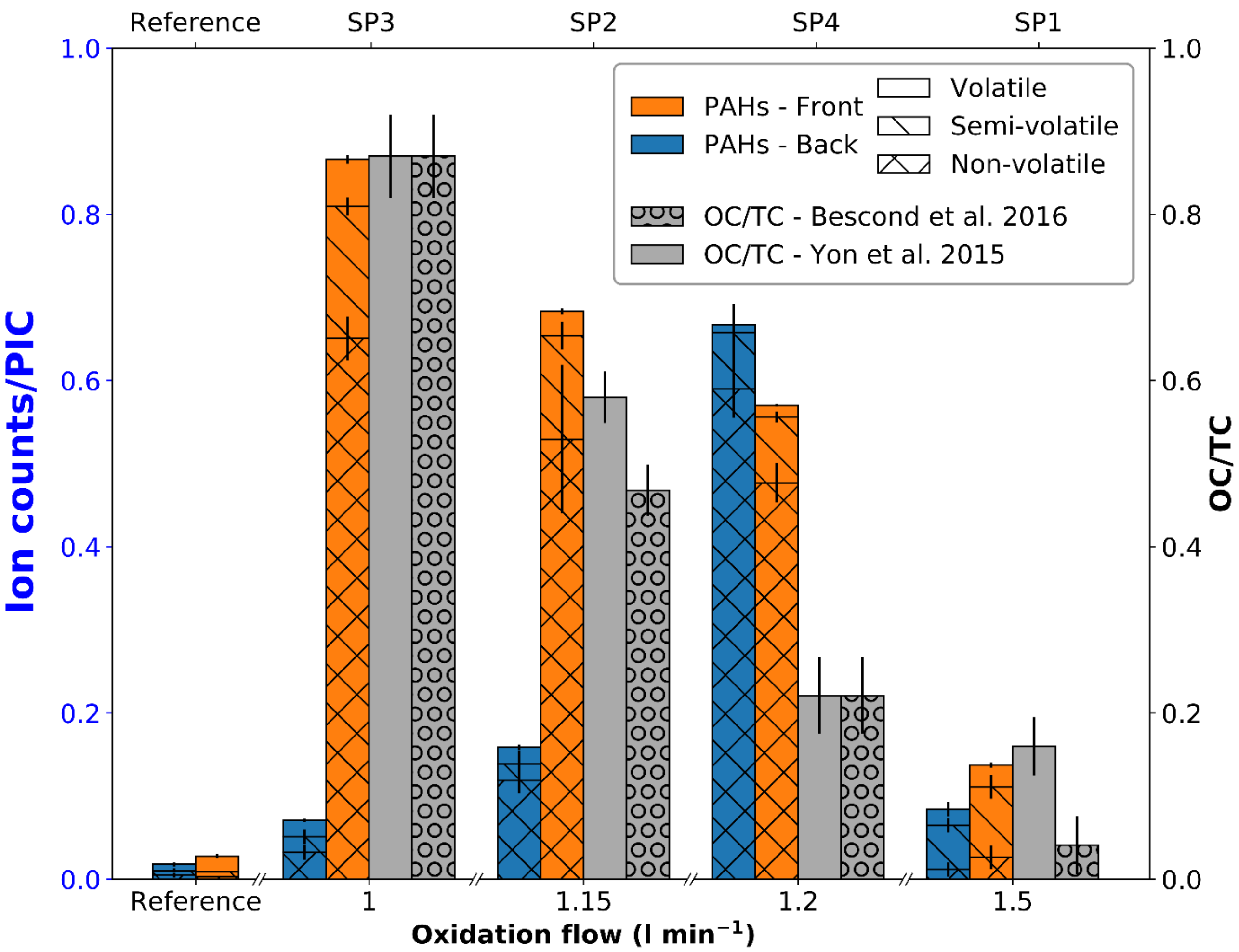

Figure 7~~6~~. Total PAH signal detected with SIMS on Front (orange) and Back (blue) Filters plotted as a function of oxidation air flow, along with OC/TC values reported in the literature for the same miniCAST set points. All values are normalized to the partial ion count (PIC) corresponding to the signal of all selected peaks.

Negative polarity mass spectra obtained for Front and Back Filters are presented in Fig. S4. H^- and C_2^- fragment ions have the highest abundance in mass spectra of $SP1_{FF}$ and $SP1_{BF}$, whereas $SP2_{FF}$, $SP3_{FF}$, $SP4_{FF}$, and $SP4_{BF}$ are dominated by H^- and C_2H^-. Similarly to that of the "reference" sample, spectra of $SP2_{BF}$ and $SP3_{BF}$ are dominated by H^- and OH^- ions. The C_nH^- series is observed in mass spectra of SP2, SP3, and SP4 samples (Front and Back Filters), with the intensity decreasing with the mass (for $n \geq 2$). To further understand this behavior, the relative abundances of the C_n^- and C_nH^- fragments are plotted as a function of the oxidation air flow in Fig. 8~~7~~. C_n^- fragments are commonly considered as markers of the EC content (Duca et al., 2019; Pagels et al., 2013; Popovicheva et al., 2017). For instance, ~~(~~Pagels et al.~~,~~ (2013)~~Pagels et al. (2013)~~ used the sum of C_n^- (n = 2–4) fragment signals as a marker of EC in aerosol time-of-flight mass spectrometer (ATOFMS) measurements for wood stove PM emissions and the same marker ions have been used to discriminate diesel from biodiesel PM emissions by Popovicheva et al. (2017). C_nH^- fragments are commonly associated with OC contents (Ewinger et al., 1991; Le Roy et al., 2015), but it is worth noticing that both series have been detected in mass spectra of pure PAHs (Bentz et al., 1995; Le Roy et al., 2015). Here, the relative proportion of C_n^- fragments increases with the initial oxidation air flow conditions on Front Filter samples and exhibits a similar contribution across Front and Back Filter samples. It should be noted also that the black carbon, pre-deposited on Back Filters, also contribute ~~also~~ to the C_n^- signal. However, for all miniCAST samples, the total C_n^- contribution is higher than that of the "reference" sample, suggesting that some proportion of C_n^- on Back Filters originates from the deposited material. On the other hand, the C_nH^- ion series shows a distribution across Front and Back samples akin to that of the total PAH signal (i.e. the total PAH signal in positive polarity, see Fig. 7~~6~~). This positive correlation indicates a possible polyaromatic origin of the C_nH^- fragments. In order to better delineate the contributions of EC, PAHs, and other components to the C_n^- carbon cluster series, Pearson correlation coefficients between all C_n^- and C_nH^- have been evaluated for the complete set of negative SIMS spectra. C_n^- (n = 1–4) ions display high positive correlation ($r \geq$ 0.60) with a maximal value for C_3^- and C_4^- (r = 0.91). In contrast~~On the contrary~~, this group of peaks is not correlated with the C_5^- fragment ion and is anticorrelated with all heavier carbon cluster ions ($n \geq 6$). This first analysis shows that at least two components contribute to the C_n^- signal. Furthermore, positive correlations are also found between the C_nH^- (n = 3–12) fragments, but also between these C_nH^- ions and the C_n^- (n = 5–12) fragments. For better visibility, specific subsets of C_n^- fragment ions (n = 1–4 and n = 5–12) are plotted separately in the lower panels of Fig. 8~~7~~. The lower left panel shows that the ions with carbon numbers n = 1–4 primarily contribute to the total C_n^- signal, whereas the lower right panel highlights the correlation between subset ions with carbon numbers n = 5–12 and C_nH^- fragments. In addition, the similar distribution across Front and Back Filters~~samples~~ between C_nH^- fragment ions and total PAH signal supports the fact that C_nH^- fragments can be considered as a marker for OC (for which PAHs are a proxy) in our soot samples. Therefore, while a predominant fraction~~part~~ of C_n^- fragments (n = 1–4) are markers for EC, a non-negligible part (C_n^- with $n \geq 5$) also originates from the organic fraction present on our samples.

SIMS results confirm L2MS measurements regarding the organic carbon and more specifically the PAH contents and mass distributions for the various miniCAST set points. In contrast to L2MS, specific SIMS fragmentation patterns provide additional information about the presence of elemental carbon and outline the distinct elemental carbon vs organic carbon contents for the different miniCAST set points.

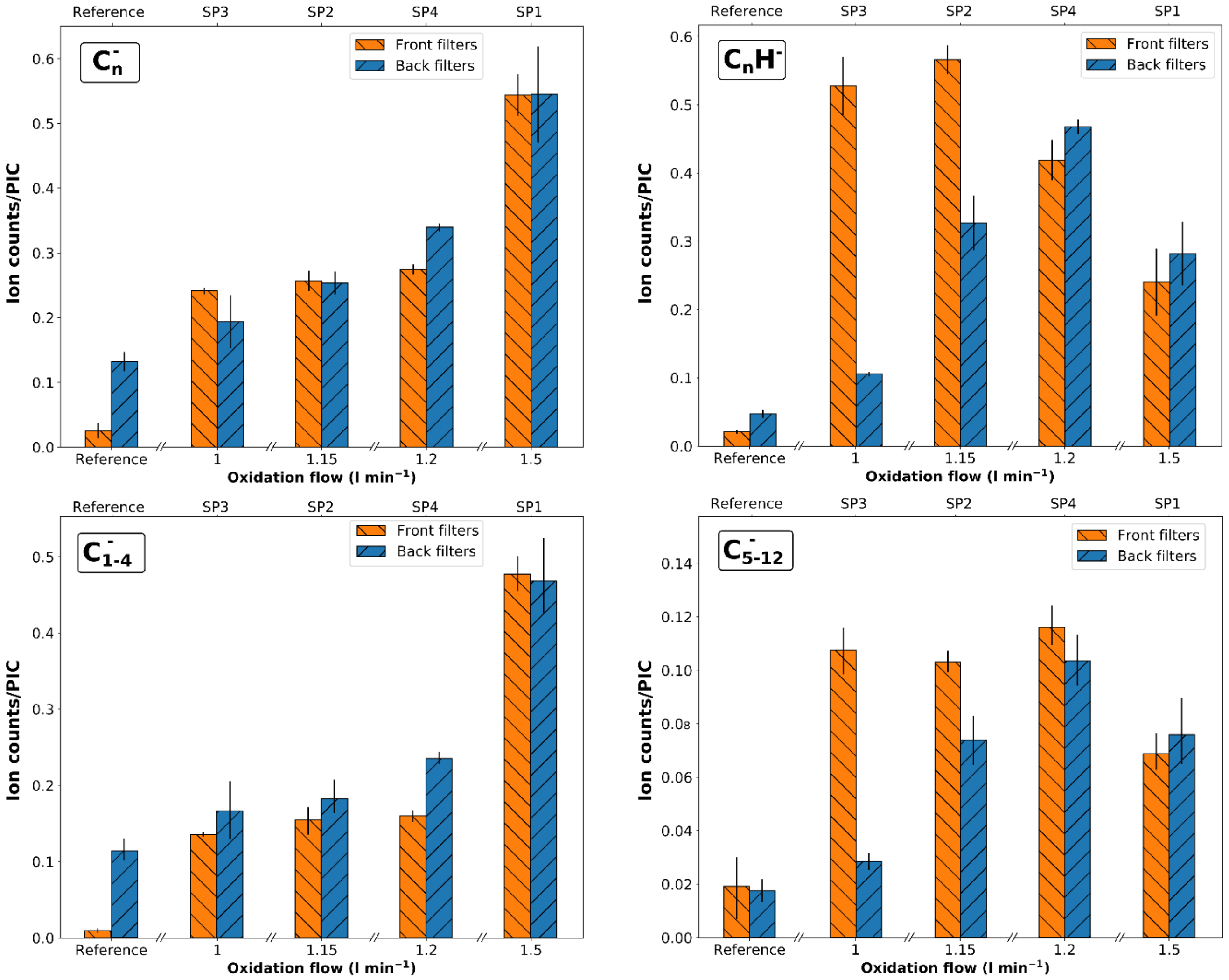

Figure 8~~7~~. Variation of the signal of various markers, as derived from SIMS spectra. The panels represent the total peak areas of the following families: (upper left) total peak area of C_n^-, (upper right) total peak area of C_nH^-, (lower left) $C_{1–4}^-$, and (lower right) $C_{5–12}^-$. All values are normalized to the partial ion count (PIC) corresponding to the signal of all selected peaks.

3.2.2 Principal component analysis of SIMS spectra

PCA was applied to the positive mode SIMS spectra. All hydrocarbon fragments and the most representative peaks for PAHs were chosen for the analysis (see Sect. S3 and Fig. S4). The PCA score plot for the first two components (PC1 and PC2, responsible for 92 % of the variance) is presented in Fig. 9~~8~~a, and their corresponding loadings in Fig. 9~~8~~c. PC1 represents 73 % of the variance and is associated with small fragment ions with $m/z < 160$ (e.g. $C_nH_3^+$ with $n = 1–3$, $C_nH_m^+$ with $m > n$,

$C_7H_7^+$, positive coefficients), and with polyaromatic species with $m/z \geq 165$ (negative coefficients). All Back Filter samples (containing gas-phase PAHs) except~~but~~ $SP4_{BF}$ have positive PC1 scores, whereas all Front Filters but $SP1_{FF}$ exhibit negative PC1 scores due to their high PAH contents. ~~$SP1_{FF}$ and $SP1_{BF}$ are located in almost the same position due to their high scores on positive PC1 that corresponds to their low-mass PAH content.~~ From this result, it can be determined that $SP3_{FF}$ has the highest relative PAH content. Among F~~f~~ront F~~f~~ilters, $SP1_{FF}$ has the smallest contribution from PAHs. $SP3_{BF}$ has the highest contribution from fragments~~,~~ associated with ~~fragmentation of~~ both aliphatic and aromatic species. The negative contribution of PC2 (19 % of the variance) is associated with the hydrogen-poor fragments ~~low-hydrogen content fragments~~ ($C_nH_m^+$ with $m < n$) and volatile and semi-volatile PAHs (m/z 128~~176~~–228) with the exception of m/z 165. The positive coefficients of PC2 are associated with aliphatic fragments (e.g. $C_nH_m^+$ with $m > n$) and large PAHs ($m/z \geq 239$). As most of the variance was contained in only two principal components (92 %), there are only two available criteria for differentiating between samples: PC1, corresponding to the amount of PAHs relative to fragments, and PC2, depending partially on ~~to~~ the hydrogen content of fragments originating from aromatic and aliphatic species. $SP1_{FF}$ and $SP1_{BF}$ are located in almost the same position due to their positive scores in PC1 and negative scores in PC2, which corresponds to their limited high-mass PAH content and high fragment content on the one hand, and small PAHs and hydrogen-rich fragments on the other hand. ~~The strong fragmentation, intrinsic to the SIMS method, is a limitation to this type of analysis. In this case, we are not able to fully differentiate between fragments coming from species with different volatility which could explain why $SP4_{BF}$ exhibits a negative PC1 score. Nevertheless, there is a notable separation between data coming from different samples, with the exception of SP1 (for the previously discussed reasons). However, there is no visible grouping for the Back/Front Filters or for the different working points.~~

~~-~~PCA was also applied to the negative mode SIMS spectra for selected mass peaks, including carbon clusters C_n^-~~, organic content markers,~~ C_nH^-, and some oxygenated and nitrogenated fragment ions. The first two components were determined to represent more than 85 % of the variance. The score plot of PC1 vs PC2 is presented in Fig. 9~~8~~b, along with their corresponding loadings (Fig. 9~~8~~d). The first component, which accounts for over 67 % of the variance, separates the samples containing low-mass carbon clusters C_n^- (with n ~~$<$~~$\leq$ 3), nitrogen and oxygen bearing compounds (e.g. CN^-, C_3NH^-, ~~HNO_3^-,~~ CH_3O^-) (positive PC1) from the samples containing species with a higher mass ($C_nH_{0-2}^-$ with $n \geq 4$~~hydrocarbons~~, oxygenated, and nitrogenated fragments – negative contribution). The opposite contributions to PC1 of small carbon clusters in comparison to larger ones, with a transition size of n = 3–4, strengthen their dichotomous origin as already discussed in Sect. 3.2.1. In the light of the score plots, $SP1_{FF}$ and $SP1_{BF}$ samples are characterized by low surface coverages where small carbon clusters are associated with the soot matrix and the black carbon respectively, whereas the other samples feature PAH-rich surfaces. PC2, accounting for 18 % of the variance, separates data points based on the contribution from hydrocarbon compounds ($C_nH_m^-$, negative PC2) and oxygen/nitrogen bearing fragments (positive contribution). ~~It is worth noting that $SP4_{FF}$ is the only front filter with a positive PC2 value, having a much more important contribution from oxygenated and nitrogenated compounds.~~ PC2 distinguishes $SP3_{BF}$, and $SP2_{BF}$ to a lesser extent, by their coverage in oxygen and nitrogen-containing species.

PCA on SIMS results confirm the existence of various families of carbon clusters on the PM that can be associated either with the soot matrix or the surface PAH coating.

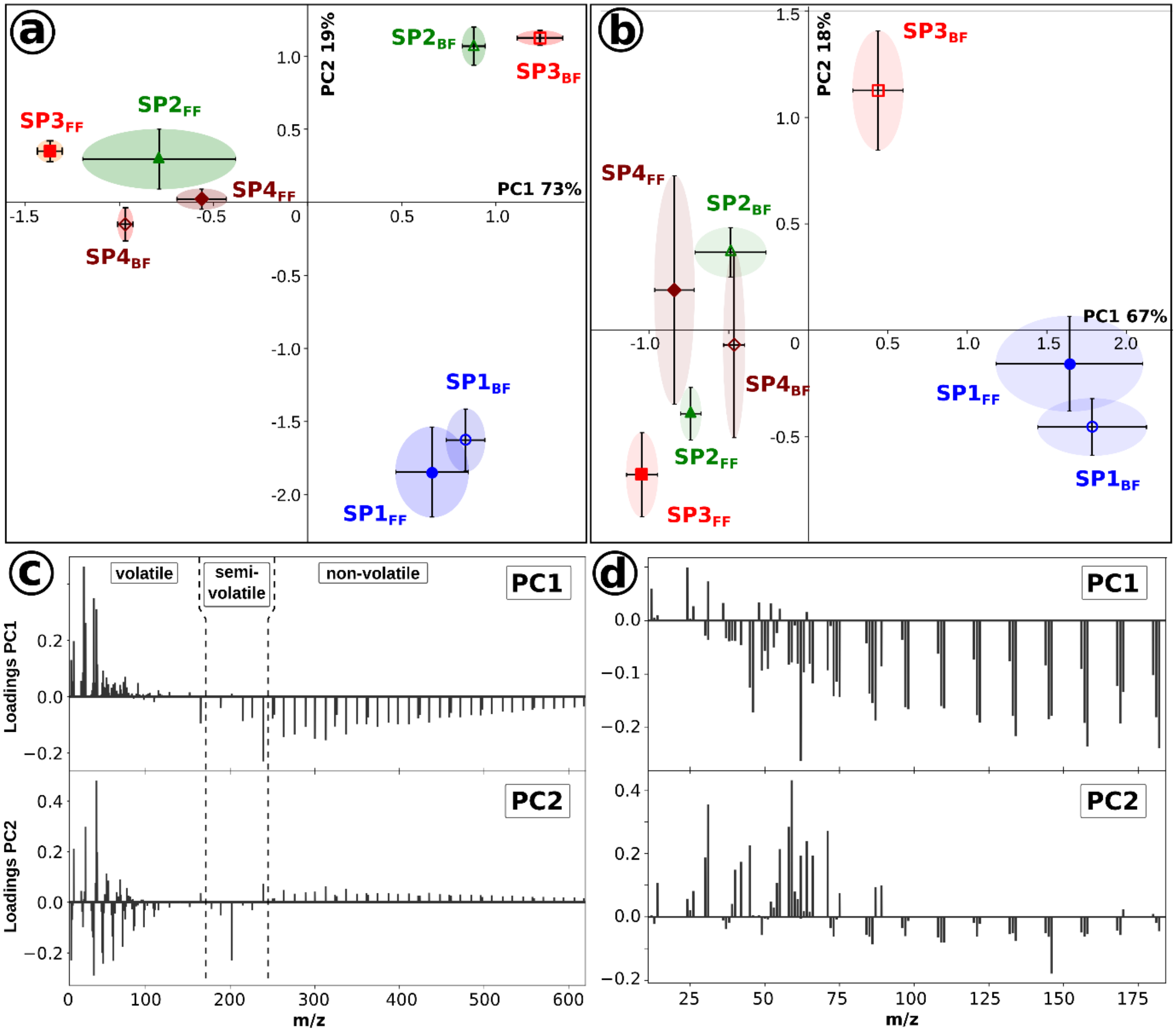

Figure 9. Score plots of PC1 and PC2 derived from positive (a) and negative (b) polarity SIMS mass spectra of miniCAST soot samples SP1, SP2, SP3, and SP4 (Front and Back Filters). Loadings corresponding to the contribution of different species to PC1 ~~(blue line)~~ and PC2 ~~(red line)~~ derived from positive (c) and negative (d) polarity SIMS mass spectra.

3.3 Raman micro-spectroscopy analysis

The two-filter system provides a unique opportunity to perform Raman spectroscopy on either the gas phase trapped on the Back Filter or the PM collected on the Front Filter. Raman spectra measured for each sample are presented in Fig. 10~~9~~. All spectra for PM deposited on Front Filters are in very good agreement with those already measured for the same miniCAST set points (e.g. Ess et al., 2016), while ~~the spectra of PM on~~ Back Filter spectra~~s~~ are dominated by the absorption of the pre-deposited black carbon. Soot particles often exhibit distinct Raman signatures that can be used to distinguish samples mostly by their hybridization and nanostructure (e.g. stacking properties) compared to that obtained for a perfect graphite crystal, i.e. a crystal made of sp^2-hybridized carbons and graphene sheets stacked with their surfaces parallel and slightly offset. When samples differ from perfect crystalline graphite, defects appear and can take the form of stacking disorder (such as in turbostratic arrangements where tortuosity reduces the stacking order), edge sites, missing atoms in the graphite lattice or even altered local or semi-long range arrangements of carbon atoms (Parent et al., 2016).

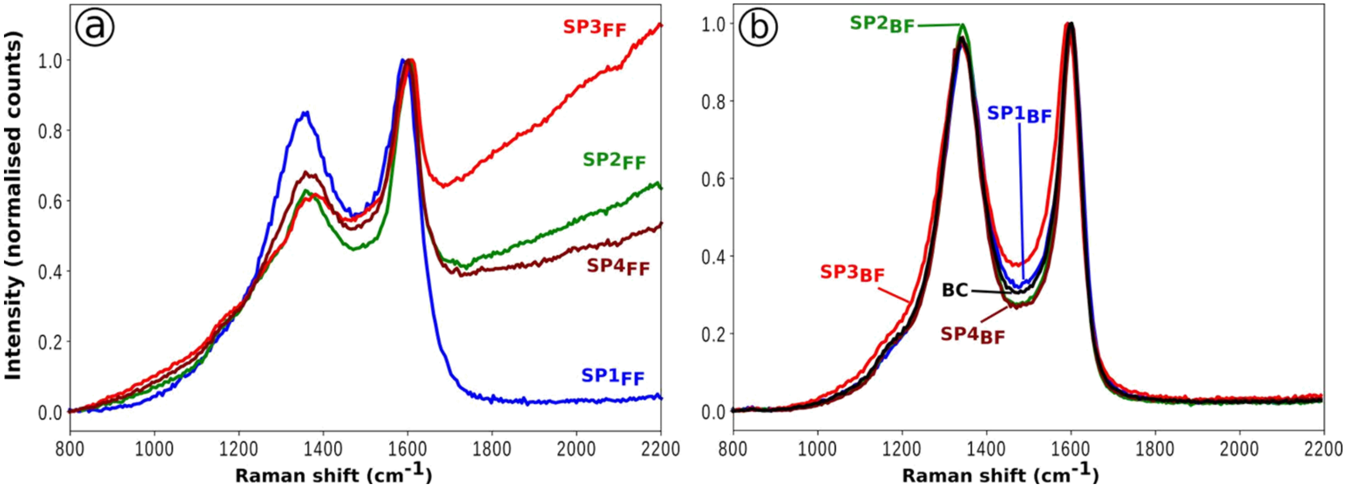

Figure 10. Raman spectra of SP1 (blue), SP2 (green), SP3 (red), and SP4 (brown) samples on Front Filter (a) and Back Filter (b). For all samples, plots are normalized to the maximum intensity of the G band. The spectrum of pure black carbon (BC) deposited on a QFF is plotted in black in panel (b) for comparison.

Both the~~ underlying~~ fluorescence background (FB) and the soot Raman feature are observed to vary significantly with the set point (Fig. 10~~9~~). The former refers to the baseline, whereas the latter refers to the two broad bands centered at 1356 cm^{-1} and 1598 cm^{-1}, termed D (for defect) and G (for graphite), which correspond to Raman scattering involving E_{2g} and A'_{1g} symmetry, respectively (Ferrari and Robertson, 2000; Sadezky et al., 2005). ~~The fluorescence background~~FB ~~(SP3 > SP2 > SP4 > SP1),~~ is attributed to surface organic content (Cloutis et al., 2016), is observed to decrease with increasing oxidation air flow for Front Filter samples ($FB_{SP3} > FB_{SP2} > FB_{SP4} > FB_{SP1}$). This trend is even clearer when the fluorescence slope fitted as a straight line between 800 and 2200 cm^{-1} (Raman shift) is plotted against the PAH signal determined in L2MS (Fig. 11~~0~~). The linear fit (R^2 = 0.992) obtained in Fig. ~~10~~ 11 reflects the good agreement between the FB~~fluorescence~~

~~background~~ and the measured trend in total PAH signal. For Back Filter samples, the FB~~fluorescence background~~ signal is nonexistent and spectra resemble that of black carbon except in the “valley” region (i.e. in between the two soot peaks).

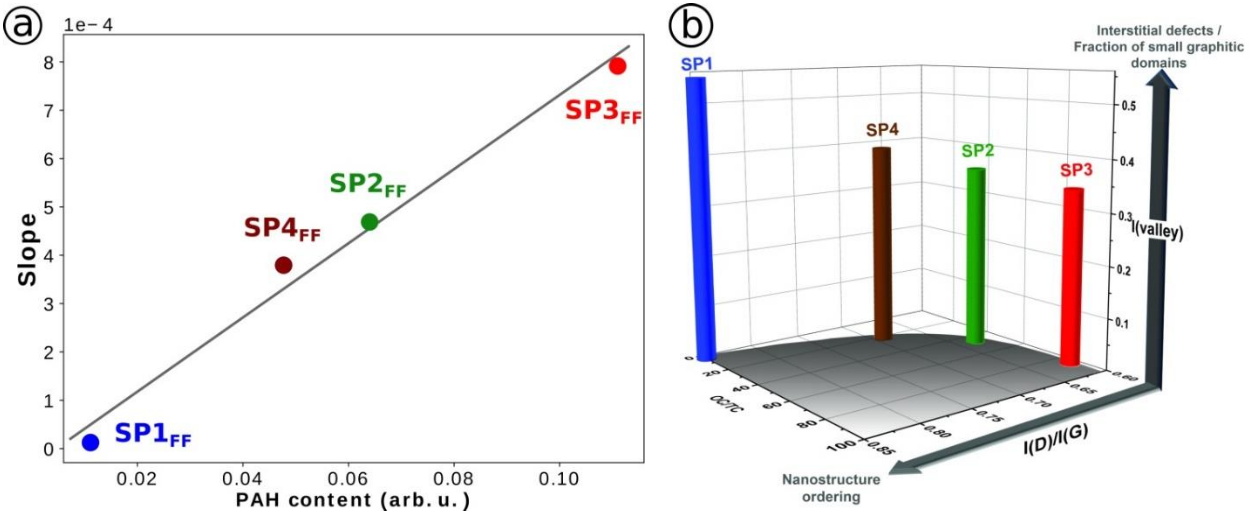

Figure 11~~0~~. (a) Fluorescence slopes extracted from Raman spectra of SP1$_{F}$~~-~~$_{F}$ - (blue), SP2$_{F}$~~-~~$_{F}$ (green), SP3$_{F}$~~-~~$_{F}$ (red), and SP4$_{F}$~~-~~$_{F}$ (brown) plotted against total PAH content measured in L2MS (in terms of ion signal) in Front Filter samples, (b) 3-D bar plot showing the evolution of the intensity of the “valley” between the two D and G bands and that of the I(D)/I(G) height-ratio with organic content (OC/TC ratio) in Front Filter samples.

Two conclusions can be drawn from these observations. First, when comparing fluorescence signals of Back and Front Filter samples to PAH content, we can further refine our definition of organic content. Fluorescence is not just related to the total PAH signal, although this is a good marker of organic content. If it were, fluorescence would also be observed for Back Filter samples, in accordance with their relatively high gas-phase PAH contents. The lack of fluorescence signal on Back Filters, whose chemical composition is dominated by small PAHs, suggests that the fluorescence can be attributed mainly to non-volatile PAHs in the particulate phase, even though the heaviest mass detected in L2MS (*m/z* 546) is still small to expect fluorescence with a 514 nm excitation wavelength (Mercier et al., 2019). Consequently, the interaction of PAHs with one another or with the PM surface seems to trigger the fluorescence excited at 514 nm. Such perturbative effect (e.g. aggregate formation) on the luminescence has been observed in solutions (Nakagawa et al., 2013).

Information on soot nanostructure ordering can be derived from the I(D)/I(G) height-ratio, whose increase in intensity reflects a higher degree of order for soot made of crystallites (L_a) smaller than 2 nm (Ess et al., 2016; Ferrari and Robertson, 2000). The height (intensity) of the valley region between the two peaks (1440–1540 cm^{-1}) provides insights into the presence of interstitial defects which may distort the lattice structure (Ess et al., 2016; Ferrari and Robertson, 2000; Sadezky et al., 2005) or into the occurrence of small graphitic domains (Parent et al., 2016). For comparison purposes, Raman spectra measured for Front Filters (Fig. 11~~0~~a) have been subsequently baseline-subtracted and normalized to the G band before interpretation. Figure 11~~0~~b shows the evolution of the I(D)/I(G) height-ratio and that of the intensity of the “valley” region with the OC/TC ratio for each set point. This 3D-bar plot confirms that the nanostructure order (I(D)/I(G) height-ratio) increases with decreasing OC content, i.e. the degree of order in the large polyaromatic network is higher under SP1 conditions (i.e. at higher oxidation air flow). This is in agreement with the analysis of Ess et al. (2016) of soot produced at set points SP1, SP2, and SP3. Furthermore, a similar behavior with the oxidation air flow has been observed through an analogous Raman tracer (AD1/(AG+AD2)) involving the integrated band areas (Carpentier et al., 2012), from soot consisting of polyaromatic units poorly linked together (analogous to SP3$_{FF}$) to soot made of cross-linked structures with aliphatic bridges (analogous to SP1$_{FF}$). Figure 11~~0~~b shows that the SP1 set~~working~~ point produces soot composed of a larger polyaromatic network (larger crystallite size) and a greater fraction of small interconnected graphitic domains (high "valley" intensity) as compared to SP3$_{FF}$. These results are in line with what has been previously observed for such miniCAST soot particles (Marhaba et al., 2019; Ouf et al., 2016), where the SP3 set point produced particles with very small crystallites (0.48–0.6 nm) and the greatest tortuosity/disordered structure (HRTEM) among all miniCAST samples.

4 Conclusions

Combustion by-products (PM and gas-phase) produced by a miniCAST generator are first separated and then characterized using a two-filter collection method and a multi-technique analytical/statistical protocol. Front and Back Filters thus generated are representative of the exhaust stream and are subsequently analyzed through first, an original L2MS technique featuring three~~3~~ ionization schemes, followed by SIMS, and last micro-Raman spectroscopy. The~~An original~~ three-wavelength L2MS scheme is employed in our study to target specific classes of compounds. On the one hand, we evidence the presence of aliphatic compounds and specific fragment ions (118 nm), and on the other hand, we can focus on aromatic species (266 nm). Aromatic species were detected in all mass spectra (L2MS and SIMS). When combined with advanced statistical methods (PCA), mass spectrometry datasets revealed how different all samples were. Based on the PAHs classification of Bari et al. (2010), we were able to discuss aromatics distribution across Front and Back Filters in terms of volatile (1–2 rings), semi-volatile (3–4 rings), and non-volatile PAHs (larger than 4 rings). We determined that PM is essentially sampled on Front Filters, whereas the dominant compounds trapped on all Back Filters were~~are~~ volatile PAHs regardless of the combustion conditions. The good separation between the two phases confirmed~~s~~ the high particle collection capability of QFF Front Filters. PCA revealed that distinct amounts of volatile compounds were present in samples produced with different combustion parameters. Specifically, changes in oxidation air flow conditions in the miniCAST resulted in notable changes in the mass distribution for both Front and Back Filters. L2MS results at 266 nm indicated that low oxidation air flow conditions (SP2 and SP3) produced more semi-volatile and non-volatile compounds in the exhaust stream. The addition of quenching gas (N_2) in the miniCAST combustion conditions (SP4) lessened the difference between Front and Back Filters which featured more homogeneous mass spectra. Complementary micro-Raman spectroscopy analyses not only confirmed the relationship between the underlying fluorescence and the total PAH signal determined by mass spectrometry, but also identified as non-volatile the nature of PAHs involved in the fluorescence and detected in the particulate phase. Finally, all analyses confirmed the validity of total PAH signal as a proxy for the organic content (OC) commonly detected in thermo-optical measurements (Bescond et al., 2016; Yon et al., 2015). Accordingly, the total PAH signal measured by mass spectrometry was observed to decrease with increasing oxidation air flow conditions in the miniCAST. The two-filter collection method in conjunction with our multi-technique analytical/statistical protocol brought~~brings~~ us closer to in-situ measurements, as the predominant chemical properties of the particles deposited on filters were~~are~~ preserved and could~~an~~ be directly compared to those determined by in-situ techniques (e.g. Ouf et al., 2016).

Data availability. The data presented here can be provided on request to the contact author.

Supplement link (will be included by Copernicus)

Author contribution. YC, CP, AF, CI, and CF conceptualized and built the sampling system and defined the methodology; LDN, YC, RI, CI, GL, and CP performed the sample collection; LDN and JAN (SIMS), DD and MV (L2MS), RI, JAN and CP (Raman) performed the analysis and data reduction; LDN, YC, DD, MV, JAN, CP, and CF interpreted the results and wrote the original draft with additional contributions from other co-authors: IKO, AF, CI, MZ, and BC. JY, ET, CI, YC and CF provided funding and access to experimental infrastructure and organized the sampling campaign. All co-authors reviewed and approved the manuscript.

Competing interests. The authors declare that they have no conflict of interest.

Acknowledgements. This work was supported by the French National Research Agency (ANR) through the PIA (Programme d'Investissement d'Avenir) under contract ANR-10-LABX-005 (CaPPA – Chemical and Physical Properties of the Atmosphere), the MERMOSE project sponsored by DGAC (French national funds), the European Commission Horizon 2020 project PEMs4Nano (H2020 Grant Agreement #724145), and the CLIMIBIO project via the Contrat de Plan É~~E~~tat-Région of the Hauts-de-France region. J.A.N. acknowledges the financial support of Horiba Scientific. The collection~~measurement~~ campaign was financed by GDR Suie (GDR CNRS 3622). The authors acknowledge N. Nuns for his support in acquiring the SIMS data.

References

An, Y. Z., Teng, S. P., Pei, Y. Q., Qin, J., Li, X. and Zhao, H.: An experimental study of polycyclic aromatic hydrocarbons and soot emissions from a GDI engine fueled with commercial gasoline, Fuel, 164, 160–171, doi:10.1016/j.fuel.2015.10.007, 2016.

Atkinson, R. and Arey, J.: Atmospheric chemistry of gas-phase polycyclic aromatic hydrocarbons: formation of atmospheric mutagens., Environ. Health Perspect., 102(suppl 4), 117–126, doi:10.1289/ehp.94102s4117, 1994.

Bandowe, B. A. M., Meusel, H., Huang, R., Ho, K., Cao, J., Hoffmann, T. and Wilcke, W.: PM2.5-bound oxygenated PAHs, nitro-PAHs and parent-PAHs from the atmosphere of a Chinese megacity: Seasonal variation, sources and cancer risk assessment, Sci. Total Environ., 473–474, 77–87, doi:10.1016/J.SCITOTENV.2013.11.108, 2014.

Bari, M. A., Baumbach, G., Kuch, B. and Scheffknecht, G.: Particle-phase concentrations of polycyclic aromatic hydrocarbons in ambient air of rural residential areas in southern Germany, Air Qual. Atmos. Heal., 3(2), 103–116, doi:10.1007/s11869-009-0057-8, 2010.

Bentz, J. W. G., Goschnick, J., Schuricht, J. and Ache, H. J.: Depth-resolved investigation of the element and compound inventory of aerosol particles from outdoor air, Fresenius. J. Anal. Chem., 353(5–8), 559–564, doi:10.1007/BF00321323, 1995.

Bescond, A., Yon, J., Ouf, F. X., Ferry, D., Delhaye, D., Gaffié, D., Coppalle, A. and Rozé, C.: Automated Determination of Aggregate Primary Particle Size Distribution by TEM Image Analysis: Application to Soot, Aerosol Sci. Technol., 48(8), 831–841, doi:10.1080/02786826.2014.932896, 2014.

Bescond, A., Yon, J., Ouf, F.-X., Rozé, C., Coppalle, A., Parent, P., Ferry, D. and Laffon, C.: Soot optical properties determined by analyzing extinction spectra in the visible near-UV: Toward an optical speciation according to constituents and structure, J. Aerosol Sci., 101, 118–132, doi:10.1016/J.JAEROSCI.2016.08.001, 2016.

Brochot, C., Abdolghader, P., Haghighat, F. and Bahloul, A.: Filtration of nanoparticles applied in general ventilation, Sci. Technol. Built Environ., 25(2), 114–127, doi:10.1080/23744731.2018.1500396, 2019.

Butcher, D. J.: Vacuum Ultraviolet Radiation for Single-Photoionization Mass Spectrometry: A Review, Microchem. J., 62(3), 354–362, doi:10.1006/MCHJ.1999.1745, 1999.

Carpentier, Y., Féraud, G., Dartois, E., Brunetto, R., Charon, E., Cao, A.-T., D’Hendecourt, L., Bréchignac, P., Rouzaud, J.-N. and Pino, T.: Nanostructuration of carbonaceous dust as seen through the positions of the 6.2 and 7.7 μ m AIBs, Astron. Astrophys., 548, A40, doi:10.1051/0004-6361/201118700, 2012.

Chazallon, B., Ziskind, M., Carpentier, Y. and Focsa, C.: CO2 Capture using semi-clathrates of quaternary ammonium salt: Structure change induced by CO2and N2 enclathration, J. Phys. Chem. B, 118(47), 13440–13452, doi:10.1021/jp507789z, 2014.

Cloutis, E., Szymanski, P., Applin, D. and Goltz, D.: Identification and discrimination of polycyclic aromatic hydrocarbons using Raman spectroscopy, Icarus, 274, 211–230, doi:10.1016/J.ICARUS.2016.03.023, 2016.

Dachs, J. and Eisenreich, S. J.: Adsorption onto aerosol soot carbon dominates gas-particle partitioning of polycyclic aromatic hydrocarbons, Environ. Sci. Technol., 34(17), 3690–3697, doi:10.1021/es991201+, 2000.

Delhaye, D., Ouf, F.-X., Ferry, D., Ortega, I. K., Penanhoat, O., Peillon, S., Salm, F., Vancassel, X., Focsa, C., Irimiea, C., Harivel, N., Perez, B., Quinton, E., Yon, J. and Gaffie, D.: The MERMOSE project: Characterization of particulate matter emissions of a commercial aircraft engine, J. Aerosol Sci., 105, 48–63, doi:10.1016/J.JAEROSCI.2016.11.018, 2017.

Duca, D., Irimiea, C., Faccinetto, A., Noble, J. A., Vojkovic, M., Carpentier, Y., Ortega, I. K., Pirim, C. and Focsa, C.: On the benefits of using multivariate analysis in mass spectrometric studies of combustion-generated aerosols, Faraday Discuss., doi:10.1039/C8FD00238J, 2019.

Elghawi, U. M., Mayouf, A., Tsolakis, A. and Wyszynski, M. L.: Vapour-phase and particulate-bound PAHs profile generated by a (SI/HCCI) engine from a winter grade commercial gasoline fuel, Fuel, 89(8), 2019–2025, doi:10.1016/J.FUEL.2010.01.002, 2010.

Ess, M. N., Ferry, D., Kireeva, E. D., Niessner, R., Ouf, F. X. and Ivleva, N. P.: In situ Raman microspectroscopic analysis of soot samples with different organic carbon content: Structural changes during heating, Carbon N. Y., 105, 572–585, doi:10.1016/j.carbon.2016.04.056, 2016.

Ewinger, H.-P., Goschnick, J. and Ache, H. J.: Analysis of organic compounds with SNMS, Fresenius. J. Anal. Chem., 341(1–2), 17–19, doi:10.1007/BF00322099, 1991.

Faccinetto, A., Thomson, K., Ziskind, M. and Focsa, C.: Coupling of desorption and photoionization processes in two-step laser mass spectrometry of polycyclic aromatic hydrocarbons, Appl. Phys. A Mater. Sci. Process., 92(4), 969–974, doi:10.1007/s00339-008-4605-0, 2008.

Faccinetto, A., Desgroux, P., Ziskind, M., Therssen, E. and Focsa, C.: High-sensitivity detection of polycyclic aromatic hydrocarbons adsorbed onto soot particles using laser desorption/laser ionization/time-of-flight mass spectrometry: An approach to studying the soot inception process in low-pressure flames, Combust. Flame, 158(2), 227–239, doi:10.1016/j.combustflame.2010.08.012, 2011.

Faccinetto, A., Focsa, C., Desgroux, P. and Ziskind, M.: Progress toward the Quantitative Analysis of PAHs Adsorbed on Soot by Laser Desorption/Laser Ionization/Time-of-Flight Mass Spectrometry, Environ. Sci. Technol., 49(17), 10510–10520, doi:10.1021/acs.est.5b02703, 2015.

Ferge, T., Karg, E., Schröppel, A., Coffee, K. R., Tobias, H. J., Frank, M., Gard, E. E. and Zimmermann, R.: Fast Determination of the Relative Elemental and Organic Carbon Content of Aerosol Samples by On-Line Single-Particle Aerosol Time-of-Flight Mass Spectrometry, Environ. Sci. Technol., 40(10), 3327–3335, doi:10.1021/es050799k, 2006.

Ferrari, A. and Robertson, J.: Interpretation of Raman spectra of disordered and amorphous carbon, Phys. Rev. B - Condens. Matter Mater. Phys., 61(20), 14095–14107, doi:10.1103/PhysRevB.61.14095, 2000.

Focsa, C., Duca, D., Noble, J. A., Vojkovic, M., Carpentier, Y., Pirim, C., Betrancourt, C., P., Desgroux, Tritscher, T., Spielvogel, J., Rahman, M., Boies, A., Lee, K. F., Bhave, A. N., Legendre, S., Lancry, O., Kreutziger, P. and Rieker, M.:

Multi-technique physico-chemical characterization of particles generated by a gasoline engine: towards measuring tailpipe emissions below 23 nm, Atmos. Environ., 2019.

Hilbig, R.: Narrowband tunable VUV radiation generated by nonresonant sum-and difference-frequency mixing in xenon and krypton, Appl. Opt., 21(5), 913–917, doi:10.1364/AO.21.000913, 1982.

Ikhenazene, R., Pirim, C., Noble, J. A., Irimiea, C., Carpentier, Y., Ortega, I. K., Ouf, F.-X., Focsa, C. and Chazallon, B.: Ice Nucleation Activities of Carbon-Bearing Materials in Deposition Mode: From Graphite to Airplane Soot Surrogates, J. Phys. Chem. C, acs.jpcc.9b08715, doi:10.1021/acs.jpcc.9b08715, 2019.

Irimiea, C., Faccinetto, A., Carpentier, Y., Ortega, I. K., Nuns, N., Therssen, E., Desgroux, P. and Focsa, C.: A comprehensive protocol for chemical analysis of flame combustion emissions by secondary ion mass spectrometry, Rapid Commun. Mass Spectrom., 32(13), 1015–1025, doi:10.1002/rcm.8133, 2018.

Irimiea, C., Faccinetto, A., Mercier, X., Ortega, I.-K., Nuns, N., Therssen, E., Desgroux, P. and Focsa, C.: Unveiling trends in soot nucleation and growth: When secondary ion mass spectrometry meets statistical analysis, Carbon N. Y., 144, 815–830, doi:10.1016/J.CARBON.2018.12.015, 2019.

Kim, K.-H., Jahan, S. A., Kabir, E. and Brown, R. J. C.: A review of airborne polycyclic aromatic hydrocarbons (PAHs) and their human health effects, Environ. Int., 60, 71–80, doi:10.1016/J.ENVINT.2013.07.019, 2013.

Lindsley, W. G.: Filter Pore Size and Aerosol Sample Collection, in NIOSH Manual of Analytical Methods (NMAM), 5th Edition, p. FP 1-14. [online] Available from: https://www.cdc.gov/niosh/docs/2014-151/pdfs/chapters/chapter-fp.pdf, 2016.

Marhaba, I., Ferry, D., Laffon, C., Regier, T. Z., Ouf, F.-X. and Parent, P.: Aircraft and MiniCAST soot at the nanoscale, Combust. Flame, 204, 278–289, doi:10.1016/j.combustflame.2019.03.018, 2019.

McLafferty, F. W. and Tureček, F.: Interpretation of mass spectra, University Science Books., 1993.

Mercier, X., Carrivain, O., Irimiea, C., Faccinetto, A. and Therssen, E.: Dimers of polycyclic aromatic hydrocarbons: the missing pieces in the soot formation process, Phys. Chem. Chem. Phys., 21(16), 8282–8294, doi:10.1039/C9CP00394K, 2019.

Mihesan, C., Ziskind, M., Therssen, E., Desgroux, P. and Focsa, C.: IR laser resonant desorption of polycyclic aromatic hydrocarbons, Chem. Phys. Lett., 423(4–6), 407–412, doi:10.1016/J.CPLETT.2006.04.032, 2006.

Mihesan, C., Ziskind, M., Therssen, E., Desgroux, P. and Focsa, C.: Parametric study of polycyclic aromatic hydrocarbon laser desorption, J. Phys. Condens. Matter, 20(2), 025221, doi:10.1088/0953-8984/20/02/025221, 2008.

Moldanová, J., Fridell, E., Popovicheva, O., Demirdjian, B., Tishkova, V., Faccinetto, A. and Focsa, C.: Characterisation of particulate matter and gaseous emissions from a large ship diesel engine, Atmos. Environ., 43(16), 2632–2641, doi:10.1016/J.ATMOSENV.2009.02.008, 2009.

Moore, R. H., Ziemba, L. D., Dutcher, D., Beyersdorf, A. J., Chan, K., Crumeyrolle, S., Raymond, T. M., Thornhill, K. L., Winstead, E. L. and Anderson, B. E.: Mapping the operation of the miniature combustion aerosol standard (Mini-CAST) soot generator, Aerosol Sci. Technol., 48(5), 467–479, doi:10.1080/02786826.2014.890694, 2014.

Mueller, L., Jakobi, G., Orasche, J., Karg, E., Sklorz, M., Abbaszade, G., Weggler, B., Jing, L., Schnelle-Kreis, J. and Zimmermann, R.: Online determination of polycyclic aromatic hydrocarbon formation from a flame soot generator Aerosols and Health, Anal. Bioanal. Chem., 407(20), 5911–5922, doi:10.1007/s00216-015-8549-x, 2015.

Munyeza, C. F., Rohwer, E. R. and Forbes, P. B. C.: A review of monitoring of airborne polycyclic aromatic hydrocarbons: An African perspective, Trends Environ. Anal. Chem., 24, e00070, doi:10.1016/j.teac.2019.e00070, 2019.

Nakagawa, K., Numata, Y., Ishino, H., Tanaka, D., Kobayashi, T. and Tokunaga, E.: Excimer luminescence from nonresonantly excited pyrene and perylene molecules in solution, J. Phys. Chem. A, 117(45), 11449–11455, doi:10.1021/jp402330n, 2013.

Nisbet, I. T. . and LaGoy, P. K.: Toxic equivalency factors (TEFs) for polycyclic aromatic hydrocarbons (PAHs), Regulatory Toxicology and Pharmacology, Regul. Toxicol. Pharmacol., 16, 290–300, 1992.

Ouf, F. X., Parent, P., Laffon, C., Marhaba, I., Ferry, D., Marcillaud, B., Antonsson, E., Benkoula, S., Liu, X. J., Nicolas, C., Robert, E., Patanen, M., Barreda, F. A., Sublemontier, O., Coppalle, A., Yon, J., Miserque, F., Mostefaoui, T., Regier, T. Z., Mitchell, J. B. A. and Miron, C.: First in-flight synchrotron X-ray absorption and photoemission study of carbon soot nanoparticles, Sci. Rep., 6, doi:10.1038/srep36495, 2016.

Pagels, J., Dutcher, D. D., Stolzenburg, M. R., Mcmurry, P. H., Gälli, M. E. and Gross, D. S.: Fine-particle emissions from solid biofuel combustion studied with single-particle mass spectrometry: Identification of markers for organics, soot, and ash components, J. Geophys. Res. Atmos., 118(2), 859–870, doi:10.1029/2012JD018389, 2013.

Pandey, S. K., Kim, K. H. and Brown, R. J. C.: A review of techniques for the determination of polycyclic aromatic hydrocarbons in air, TrAC - Trends Anal. Chem., 30(11), 1716–1739, doi:10.1016/j.trac.2011.06.017, 2011.

Paolini, V., Guerriero, E., Bacaloni, A., Rotatori, M., Benedetti, P. and Mosca, S.: Simultaneous Sampling of Vapor and Particle-Phase Carcinogenic Polycyclic Aromatic Hydrocarbons on Functionalized Glass Fiber Filters, Aerosol Air Qual. Res., 16(1), 175–183, doi:10.4209/aaqr.2015.07.0476, 2017.

Parent, P., Laffon, C., Marhaba, I., Ferry, D., Regier, T. Z., Ortega, I. K., Chazallon, B., Carpentier, Y. and Focsa, C.: Nanoscale characterization of aircraft soot: A high-resolution transmission electron microscopy, Raman spectroscopy, X-ray photoelectron and near-edge X-ray absorption spectroscopy study, Carbon N. Y., 101, 86–100, doi:10.1016/j.carbon.2016.01.040, 2016.

Popovicheva, O. B., Irimiea, C., Carpentier, Y., Ortega, I. K., Kireeva, E. D., Shonija, N. K., Schwarz, J., Vojtíšek-Lom, M.

and Focsa, C.: Chemical composition of diesel/biodiesel particulate exhaust by FTIR spectroscopy and mass spectrometry: Impact of fuel and driving cycle, Aerosol Air Qual. Res., 17(7), 1717–1734, doi:10.4209/aaqr.2017.04.0127, 2017.

Ravindra, K., Bencs, L., Wauters, E., De Hoog, J., Deutsch, F., Roekens, E., Bleux, N., Berghmans, P. and Van Grieken, R.: Seasonal and site-specific variation in vapour and aerosol phase PAHs over Flanders (Belgium) and their relation with anthropogenic activities, Atmos. Environ., 40(4), 771–785, doi:10.1016/j.atmosenv.2005.10.011, 2006.

Le Roy, L., Bardyn, A., Briois, C., Cottin, H., Fray, N., Thirkell, L. and Hilchenbach, M.: COSIMA calibration for the detection and characterization of the cometary solid organic matter, Planet. Space Sci., 105, 1–25, doi:10.1016/j.pss.2014.08.015, 2015.

Sadezky, A., Muckenhuber, H., Grothe, H., Niessner, R. and Pöschl, U.: Raman microspectroscopy of soot and related carbonaceous materials: Spectral analysis and structural information, Carbon N. Y., 43(8), 1731–1742, doi:10.1016/j.carbon.2005.02.018, 2005.

Stein, S. E. and Fahr, A.: High-temperature stabilities of hydrocarbons, J. Phys. Chem., 89(17), 3714–3725, doi:10.1021/j100263a027, 1985.

Sun, P., Blanchard, P., Brice, K. A. and Hites, R. A.: Trends in Polycyclic Aromatic Hydrocarbon Concentrations in the Great Lakes Atmosphere, Environ. Sci. Technol., 40(20), 6221–6227, doi:10.1021/es0607279, 2006.

Szulejko, J. E., Kim, K. H., Brown, R. J. C. and Bae, M. S.: Review of progress in solvent-extraction techniques for the determination of polyaromatic hydrocarbons as airborne pollutants, TrAC - Trends Anal. Chem., 61, 40–48, doi:10.1016/j.trac.2014.07.001, 2014.

Villanueva, F., Sevilla, G., Lara, S., Martín, P., Salgado, S., Albaladejo, J. and Cabañas, B.: Application of gas chromatography coupled with tandem mass spectrometry for the assessment of PAH levels in non industrial indoor air, Microchem. J., 142, 117–125, doi:10.1016/J.MICROC.2018.06.021, 2018.

Yon, J., Bescond, A. and Ouf, F. X.: A simple semi-empirical model for effective density measurements of fractal aggregates, J. Aerosol Sci., 87, 28–37, doi:10.1016/j.jaerosci.2015.05.003, 2015.

Yon, J., Ouf, F. X., Hebert, D., Mitchell, J. B., Teuscher, N., Garrec, J. L. Le, Bescond, A., Baumann, W., Ourdani, D., Bizien, T. and Perez, J.: Investigation of soot oxidation by coupling LII, SAXS and scattering measurements, Combust. Flame, 190, 441–453, doi:10.1016/j.combustflame.2017.12.014, 2018.

Zíková, N., Ondráček, J. and Ždímal, V.: Size-Resolved Penetration Through High-Efficiency Filter Media Typically Used for Aerosol Sampling, Aerosol Sci. Technol., 49(4), 239–249, doi:10.1080/02786826.2015.1020997, 2015.